remote sensing

MDPI

Article

Development of a UAV Based Framework for CH_4 Monitoring in Sludge Treatment Centres

Hiniduma Gamage Kavindi Abeywickrama [1], Yadira Bajón-Fernández [1], Bharanitharan Srinamasivayam [2], Duncan Turner [2] and Mónica Rivas Casado [1,*]

[1] School of Water, Energy and Environment, Cranfield University, Cranfield MK43 0AL, UK; k.a.hinidumagamage@cranfield.ac.uk (H.G.K.A.); y.bajonfernandez@cranfield.ac.uk (Y.B.-F.)
[2] Severn Trent Water, 2 St Johns St, Coventry CV1 2LZ, UK; bharanitharan.srinamasivayam@severntrent.co.uk (B.S.); duncan.turner@severntrent.co.uk (D.T.)
* Correspondence: m.rivas-casado@cranfield.ac.uk

Abstract: With the increasing trend in the global average temperature, the UK's water industry has committed to achieve Net Zero by 2030 and part of this includes cutting CH_4 emissions from sludge treatment facilities. Currently, emissions are estimated following the carbon accounting workbook guidelines and using default emission factors. However, this method might not be a true representation of emissions as these vary depending on many factors. The use of unmanned aerial vehicles (UAVs) has proved cost effective for environmental monitoring tasks requiring high spatial resolution information. Within the context of CH_4 emissions and in the last decade, the technology has been curtailed by sensor weight and size. Recent advances in sensor technology have enabled the development of a fit-for purpose UAV CH_4 sensor (U10) which uses Tuneable Diode Laser Absorption Spectroscopy. This study intends to develop a framework for CH_4 data collection strategies from sludge treatment centres using UAV-U10 technology and asset level CH_4 enhancement estimations based on geostatistical interpolation techniques and the mass balance approach. The framework presented here enables the characterization of spatial and temporal variations in CH_4 concentrations. It promotes asset level CH_4 enhancement estimation based on on-site measurements.

Keywords: sludge treatment centre; UAV; open-path TDLAS; enhancement estimation

check for updates

Citation: Abeywickrama, H.G.K.; Bajón-Fernández, Y.; Srinamasivayam, B.; Turner, D.; Rivas Casado, M. Development of a UAV Based Framework for CH_4 Monitoring in Sludge Treatment Centres. *Remote Sens.* **2023**, *15*, 3704. https://doi.org/10.3390/rs15153704

Academic Editor: Richard Becker

Received: 7 June 2023
Revised: 11 July 2023
Accepted: 18 July 2023
Published: 25 July 2023

1. Introduction

Under the 2016 Paris agreement [1], the United Nations Framework Convention on Climate Change (UNFCCC) sets their target on maintaining global average temperature increment to be below 2 °C. This requires countries to reduce their greenhouse gas (GHG) net emissions by 100% by 2050 [1]. The UK has started working towards achieving carbon Net Zero by 2050 as recommended by the Committee on Climate Change (CCC) [2]. The UK water industry is committed to achieve Net Zero carbon emissions by 2030 and is currently progressing towards it [1]. In 2020, GHG emission of waste management which consists of waste disposed to landfills, waste incineration and wastewater treatment (WWT) reported 4% of the UK's GHG emissions [3]. As a result, companies operating wastewater treatment plants (WWTPs) have been focusing on the development and implementation of GHG monitoring and quantification methods. CH_4 quantification has become key in this process, as it is the major contributor to GHG emission when it comes to sludge treatment centres, where the main byproduct of WWT process is treated [3]. Currently, CH_4 emissions are quantified following the carbon accounting workbook (CAW) guidelines and their fixed emissions factors (EFs) [4], but concerns have arisen to which extent these EFs are realistic as asset specific EFs depend on operational activities, meteorological conditions and site geography, amongst other variables.

CH_4 can be emitted at different stages by different assets in the sludge treatment process. For example, the anaerobic digesters and partially processed sludge will lead to CH_4 emission in digestate storage tanks, where tanks with more than 1 m depth have a higher chance of emitting CH_4 [5]. The level of emission will also vary from plant to plant depending on age, type of asset and treatment process. Therefore, it is essential to monitor CH_4 emission at each stage in the WWT process at each plant to identify possible sources, reliably estimate asset specific CH_4 emissions and develop informed management decisions.

In a previous study by Daelman et al. [6], CH_4 emission estimates in WWTPs were determined using flowrates in pipelines and analysing samples from gasbags. The salting-out method was used to sample dissolved CH_4. In recent studies, remote sensing methods coupled with the mass balance approach [7–9] or the tracer gas dispersion method [10] have been used to estimate CH_4 emission. Delre et al. [10] used the tracer gas dispersion method and a remote sensing-based methodology to estimate CH_4 emissions in five WWTPs. The proposed methodology required an initial site screening in order to find out any potential emission sources. The authors concluded that plant specific EFs obtained for these WWTPs were varied; EFs were lowest in plants with enclosed sludge treatment and storage units. The use of remote sensing methods leads to more reliable estimations when compared with more traditional methods (i.e., default EFs) since remote sensing enables the identification and inclusion of additional emission sources within the plant.

Quantification of CH_4 in WWTPs is difficult as it requires sampling of relatively large areas with multiple potential CH_4 sources in close proximity. Robust quantification of CH_4 emission from individual assets with ground-based sensors is challenging, unless these sensors are installed at multiple heights and at a relatively high spatial sampling density within the plant. This requires significant investment in sensor acquisition and deployment, in addition to high maintenance costs and human resources. Unmanned aerial vehicles (UAVs) have proven to be an effective tool for environmental monitoring, including air pollution [11], enabling wide-area and on-demand data collection whilst minimizing operational costs and the need for human resources. The main advantages of UAV based sensors over ground-based portable sensors are: (i) being able to monitor concentrations at different heights, close to the source and with a high spatial resolution within a short period of time, and (ii) being able to access areas which are risky for human to access [12]. Previous research has explored the integration of sensors into UAV platforms for CH_4 monitoring purposes. Allen et al. [8] used a vertical take-off and landing (VTOL) UAV DJI F550 and a fixed wing UAV to observe the ratio between carbon dioxide (CO_2) and CH_4 and quantify CH_4 emissions in a landfill, respectively. At that time, there were no suitable sensors fulfilling the requirements to mount on-board the VTOL platform. Therefore, a tethered sampling line (Teflon tube) connected to the power supply line and to a gas analyser on the ground which could measure both CO_2 and CH_4 was used. The flight radius was limited by the tether, but it allowed unlimited endurance due to the continuous power supply. The fixed wing UAV had an on-board non-dispersive infrared (NDIR) sensor which measured CO_2 and captured the spatial extent of the CH_4 plume using the characterized ratio with the data observed by the VTOL. The authors estimated CH_4 flux using the mass balance approach. In their study, Kriging geostatistical techniques [13] were used to interpolate CH_4 measurements to the plane of interest for the implementation of the mass balance approach. Kriging interpolation was considered essential to generate the continuous surface of CH_4 measurements required by the mass balance. Both UAVs were deployed at the same time to quantify both gases simultaneously. When using the mass balance approach, CH_4 is quantified in a 2D plane perpendicular to the prevailing wind direction. The fixed wing was flown both in horizontal and vertical directions resulting in a 3D configuration which was later projected on to a 2D plane. The use of the sampling technology and emission estimations was linked to different sources of errors. For example, the racetrack width should have been minimized to increase the estimated flux accuracy. The use of the characterized ratio and CO_2 levels to estimate CH_4 concentrations also added an error to the flux estimation. The need for further studies that look at using sensors that provide direct CH_4 measurements was identified. Nathan et al. [7] used an open-path tuneable diode laser absorption spectroscopy (TDLAS) sensor mounted on a fixed wing to collect vertical path integrated CH_4 measurements. The authors also relied on the mass balance approach and Kriging interpolation to estimate emissions of CH_4 mass fluxes from a compressor station.

Yang et al. [9] used a VTOL UAV to estimate CH_4 flux from well pads. The platform had an on-board open-path TDLAS sensor to measure vertical path integrated CH_4 concentrations. The flux was estimated using the mass balance approach. Here, the racetrack width was minimized since, unlike the fixed wing, the VTOL can change flight direction instantly. Vertical flightpaths were not necessary since the sensor gave the vertical path integrated concentrations when the laser was maintained in nadir position.

There are not many commercial sensors that have achieved the required miniaturization. Open-path TDLAS sensors have achieved this. TDLAS technology emerged in the 1990s and it was recently miniaturized to mount on-board small UAVs. Tokyo Gas Engineering Co. Ltd. made the sensor commercially available in 2013. At the time, the sensor could detect path integrated CH_4 concentrations ranging from 1–50,000 ppm·m with a response time of 0.1 s and detection distance ranging from 0.5–30 m [14]. In 2019, AiLF partnered with DJI and released the U10, a more advanced open-path TDLAS sensor [15]. This technology avoids the need of in-situ measurements and does not require for the sensor to be located at the point of interest to take the measurement. To date, the use of the U10 for path integrated CH_4 concentrations monitoring in WWTP is unexplored. The aim of this paper is to develop UAV-U10 data collection strategies for vertical path integrated CH_4 concentrations in closed (anaerobic digesters) and open (cake pads and digestate storage tanks) WWT assets in a selected sludge treatment centre. This will be achieved through the following objectives.

Objective 1. *To characterize vertical path integrated CH_4 concentrations for anaerobic digesters, digestate storage tanks and cake pad assets in a selected WWTP.*

Objective 2. *To estimate CH_4 enhancement from the assets considered under Objective 1.*

Objective 3. *To interpret the results from Objective 1 and Objective 2 within the context of path integrated CH_4 concentration monitoring for Net Zero compliance.*

2. Materials and Methods

2.1. Selection of the Case Study Area and WWTP Assets

A WWTP with a sludge treatment centre at Minworth (West Midlands, UK) was selected as the case study area (Figure 1). Three main criteria were behind the selection: size, roadmap to Net Zero targets and existing asset combination. GHG emissions at Minworth are expected to be of more significance than in other WWTPs as it is the second largest plant in the UK, capable of serving a population of ≈1.7 million [16].

Minworth WWTP is already working towards achieving the Net Zero targets and implementing the 2030 route map. Therefore, a plan is already in place to integrate technological advances that contribute to achieve 2030 Net Zero goals. The WWTP presents a wide range of WWT assets (Figure 1). This study focuses on the monitoring of CH_4 for anaerobic digesters, digestate storage tanks and sludge cake pads. These assets were selected because they are the major contributors of CH_4.

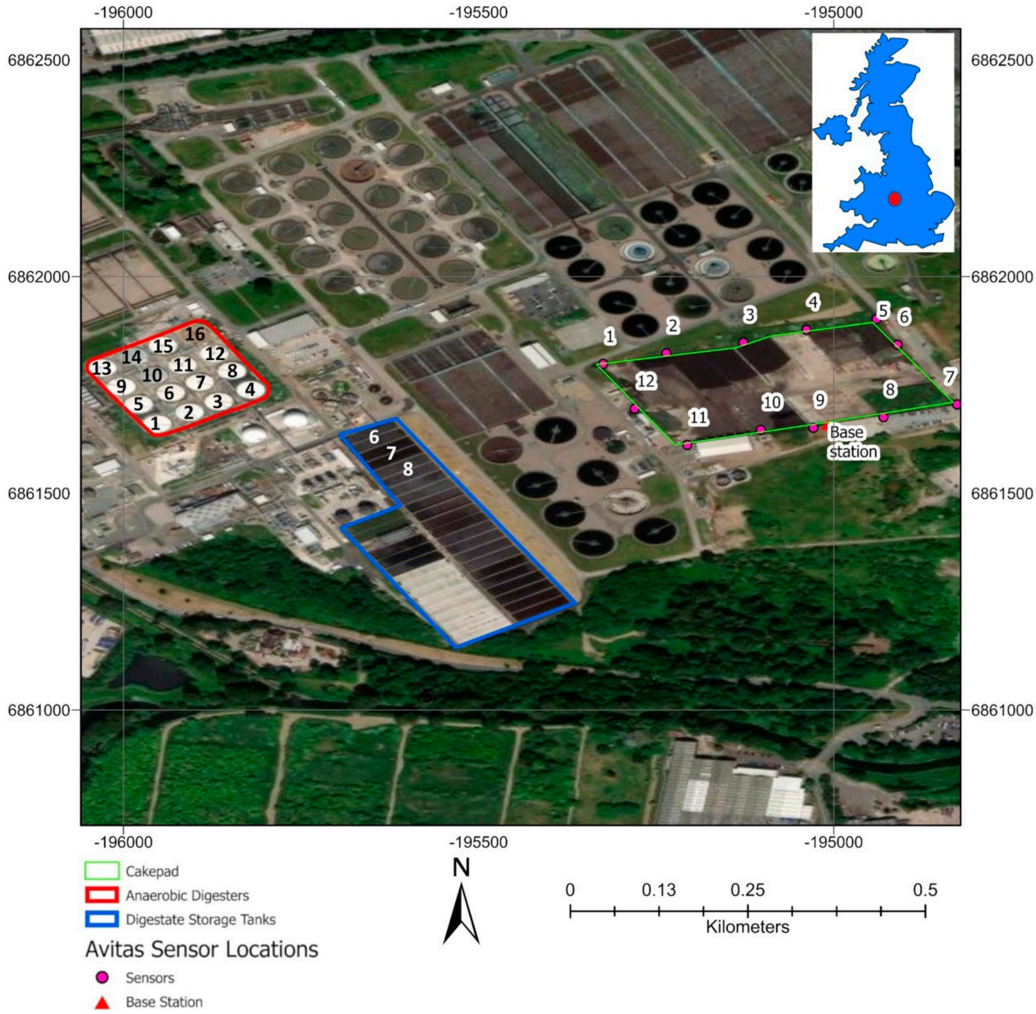

Figure 1. Maps showing the location and distribution of the sludge treatment assets at Minworth WWTP (numbers identify ground sensors along the cake pad area (green polygon) and single units within digestate storage tanks (blue) and anaerobic digesters (red)): generated using ArcGIS Pro 2.8 (Esri, Redlands, CA, USA). Source: [17].

Within the WWTP, there are sixteen anaerobic digesters, of which only fourteen were functional (all except digesters 12 and 16) for the duration of the study (Figure 1). They are cylindrical in shape with a height above the ground of 10 m and 26 m of diameter. The digesters are evenly distributed within a 125 m × 125 m area, with their centres 27 m apart from each other. They receive 100% of the sludge volume produced in the WWTP (approximately 71,700 tDS annually) (Severn Trent Water, Coventry, UK, personal comment).

The digestate storage tanks are open tanks and they extend over an L-shape area where longer length, shorter length and width are approximately 360 m, 300 m and 160 m, respectively (Figure 1). There are sixteen rectangular open storage tanks (55 m × 26 m) separated by solid concrete walls, each having two bays of equal size separated by arched concrete walls.

The cake pads extend for an area of ≈300 m × 150 m (Figure 1). There are sixteen bays separated by solid concrete walls. The length and width of a single bay are approximately 60 m and 26 m, respectively. There is a central reservation between upper eight bays and lower eight bays for cake movement and transport purposes. The plant produces approximately an average of 36,000 tDS of treated cake and 100% of sludge cake produced goes to land (Severn Trent Water, personal comment).

The plant operates 24/7 at a constant production rate. However, it receives greater sludge volume during autumn and winter when increased rainfall events result in more surface run-off and drainage water to the plant.

2.2. Selection of UAV Platform and CH_4 Sensor to Be Mounted Onboard

There are mainly two types of UAVs, namely, fixed wings and VTOLs. A bespoke deployment platform is needed for fixed wing UAVs to take off and a racetrack to safely land. VTOLs are easier to deploy as they are able to take-off and land vertically. VTOLs can be easily operated to fly in any direction and are capable of hovering over a designated landmark. Therefore, they are preferred in applications requiring close-to-source monitoring.

There are different types of sensors with different sensing mechanisms for CH_4 quantification which can be mounted on-board of an UAV. They are same as the sensors used for ground-based monitoring but they require miniaturization since weight and size of the sensor are generally critical constraints curtailing integration. Non-optical based sensors are low cost and light weight, and may be preferred for integration into UAV platforms. However, they are less sensitive and cross-sensitive to other trace gases, leading to inaccurate measurements and therefore making them less suitable than optical sensors for monitoring purposes [18].

There are miniaturized NDIR sensors which can be mounted on small UAVs and they are less expensive compared to other optical sensors. Shah et al. (2019) [12] used a NDIR sensor mounted on-board a UAV to estimate CH_4 flux. Its nominal power consumption, weight and dimensions are 4.2 W, 327 g and L 220 $\times$ W 110 $\times$ H 75 mm, respectively. In their study, flux calculations failed because the sensor was not able to accurately measure background concentrations due to a high signal-to-noise ratio. The authors suggested that the sensor could be used to measure CH_4 enhancements in the order of 10 ppm and concluded that simple spectroscopic techniques such as NDIR are not suitable for deriving accurate and reliable CH_4 measurements on-board a UAV.

Cavity ring down spectroscopy (CRDS) sensors have high sensitivity when compared with NDIR and TDLAS sensors since the laser path length through the gas sample is greater as it reflects back and forth inside the chamber [19]. However, a CRDS sensor mounted onboard a UAV platform requires data collection at different heights as it only detects in-situ measurements. Additionally, CRDS sensors are heavier compared to open-path TDLAS, and would require a UAVs capable of lifting such payloads, although they would provide higher accuracy [19,20]. Compared to commercially available heavy lifting UAVs (e.g.,: M600 Pro, DJI, Shenzhen, China), the UAV used in this study (Matrice 300 RTK, DJI, Shenzhen, China) has enhanced flight time, maximum flying speed, wind resistance and maximum transmission range [21,22]. Therefore, the U10 open-path TDLAS sensor mounted on the Matrice 300 RTK (DJI, Shenzhen, China) platform was selected for data collection purposes in this study.

2.3. Data Collection

2.3.1. UAV Data Collection

The Matrice 300 RTK (DJI, Shenzhen, China) integrated with a U10 open-path TDLAS CH_4 sensor (Figure 2) was used to measure vertical path integrated CH_4 concentration. The Matrice 300 (DJI, Shenzhen, China) is a 0.8 m $\times$ 0.7 m VTOL quadcopter powered by a TB60 LiPO 12S battery of 5935 mAh of capacity (1.35 kg), with a maximum take-off weight of 9 kg. The vision systems of the Matrice 300 have an obstacle sensing range of 0.7–40 m (forward/backward/left right) and 0.6–30 m (upward/downward). The platform is equipped with a GNSS GPS Glonsas, BeiDou and Galileo positioning system that provides an accuracy of up to 1 cm + 1 ppm in planimetry and 1.5 cm + 1 ppm in altimetry. The hovering accuracy of the platform when the RTK GPS is enabled is 0.1 m in both planimetry and altimetry. The operational range and more general characteristics of the platform are described in Table 1. The U10 TDLAS sensor uses CH_4 absorption spectroscopy to quantify CH_4 using the Beer–Lambert Law, which states that absorption of light by the gas is proportional to the concentration and path length through the plume of the specific gas [15]. The U10 threshold of detection is 5 ppm·m and points with emissions below the threshold are not logged in by the system.

Figure 2. Equipment used. (**a**) Matrice 300 RTK DJI UAV (DJI, Shenzhen, China) equipped with the U10 sensor. (**b**) Calibration cell unit; a standard gas sample of CH_4 of 1700 ppm·m ± 10%.

Table 1. DJI Matrice 300 RTK UAV platform (DJI, Shenzhen, China) [21] and U10 sensor [15] specifications.

Platform Specifications	
Maximum flight time	55 min (no payload), 33 min (maximum payload)
Transmission range	15 km
Transmission frequency	2.4–5.8 GHz
Maximum descend speed	7 m s^{-1}
Maximum speed	23 m s^{-1}
Wind resistance	15 m s^{-1}
Maximum payload capacity	2.7 kg (mount up to 3 payloads)
Operating temperature	−20 °C to 50 °C
Volume	L 810 × W 670 × H 430 mm (unfolded, propellers excluded)
Weight	Approximately 3.6 kg (without batteries)
Sensor Specifications	
Detection laser	Class IIIR
Static detection limit	5 ppm·m
Sampling frequency	500 kHz
Response time	0.025 s
Measuring range	0–50,000 ppm·m
Maximum distance	100 m
Working temperature	−20–50 °C
Operating humidity	<90% relative humidity
Volume	L 155 × W 90 × H 100 mm
Weight	520 g

Data were collected when suitable meteorological and site conditions were met. Within this context, suitable meteorological conditions were considered to be sunny days with prevailing visibility up to 10,000 m AMSL, no clouds and stable wind conditions below 6 m s^{-1}. Each asset was surveyed through consecutive flight missions and full spatial coverage was ensured through the combination of multipasses. In addition to path integrated CH_4 concentration, the Matrice 300 also recorded wind speed and direction at ground level, as well as flight altitude. Wind data were derived from an onboard software. Each flight was conducted within 30 min, with all the missions per asset taking between 4 to 5 h to be completed (Table 2). Small variations in flight plan arrangements were implemented per asset as required. The platform was flown under manual mode by a fully qualified pilot and following Civil Aviation Authority regulation at all times. Take-off and landing were automated for safety purposes. Vertical path integrated CH_4 concentration was measured every 2 m along each flight pass with the U10 pointing in nadir position. The accuracy of the U10 was verified before each survey to assess whether re-calibration was required. For that purpose, a calibration cell was used as a standard gas sample to check if the accuracy of U10 measurements were within the expected range (Figure 2). The U10 sensor was sent for calibration to DJI's factory when required by the scheduled calibration timeline or when the device indicated the need for a check [12].

Table 2. Summary of survey characteristics and ancillary data collected for each asset. Wind direction is represented following UK Met Office format (e.g., northerly winds—360°, southerly winds—180°, westerly winds—270°, easterly winds—90°). $\overline{W}$, $\overline{WD}$, $\overline{P}$, $\overline{T}$ and $\overline{RH}$ stand for mean wind speed, mean ground wind direction, mean ground pressure, mean ground temperature and ground relative humidity, respectively per survey with standard deviation. For digestate storage tanks, data collection was done within a single mission (second mission). All CH_4 measurements for the cake pad survey were below quantification level when the laser was in the nadir position. The number of CH_4 points represents the readings after excluding isolated measurements. AD, DST and CP stand for anaerobic digesters, digestate storage tanks and cake pads, respectively.

Survey Description					
Asset	**Date**	**N° Missions**	**Area (m^2)**	**N° CH_4 Points**	**Effective Surveying Time (h)**
AD	21 March 2022 18 May 2022	6 8	22,500 22,500	3771 284	4.5 5.5
DST	4 November 2022	1	1430	532	0.3
CP	18 March 2022	3	1560	-	0.5
UAV ancillary data					
Asset	**$\overline{W}$ (m s^{-1})**	**$\overline{WD}$ (°)**	**$\overline{T}$ (°C)**	**$\overline{RH}$ (%)**	**$\overline{P}$ (hPa)**
AD	2.7 ± 0.1 4.7 ± 0.1	151 ± 9 194 ± 5	12.7 ± 0.7 18.0 ± 1.4	59 ± 4 58 ± 3	1025.8 ± 0.4 1018.3 ± 1.2
DST	4.9	302	12.3	72	1013.8
CP	N/A	N/A	N/A	N/A	N/A
Metal oxide ground sensor data					
Asset	**$\overline{W}$ (m s^{-1})**	**$\overline{WD}$ (°)**	**$\overline{T}$ (°C)**	**$\overline{RH}$ (%)**	
AD	1.00 ± 0.01 0.88 ± 0.01	117 ± 21 164 ± 36	12.6 ± 1.2 22.5 ± 1.4	64 ± 2 62 ± 4	
DST	0.130 ± 0.001	311 ± 15	11.8 ± 0.4	75 ± 1	
CP	2.01 ± 0.04	126 ± 21	15.9 ± 0.5	64 ± 2	

The anaerobic digesters were surveyed on 21 March 2022 (4.5 h of survey time) and on 18 May 2022 (5.5 h). Herein after, mission refers to each flight from take-off to landing conducted within a survey day. On 21 March 2022 (6 missions), the flight plan covered the full extent of the asset in addition to a 25 m buffer around the perimeter. The width of the buffer was determined based on the proximity of the asset to adjacent gas bags and roads. The total area surveyed was ≈22,500 m^2. The flight plan consisted of diagonal multipasses spaced 2 m from each other (Figure 3). The buffer area was surveyed after surveying the individual digesters. Vertical path integrated CH_4 concentration was measured every 2 m with the U10 laser maintained in nadir position. The flight altitude was maintained constant at 30 m from the top of the digester. Lessons learnt during the first survey informed the next survey. On 18 May 2022, both the anaerobic digesters and the buffer were surveyed twice following diagonal transects (Figure 3). A total of 8 missions were required to cover the full extent. The same flight parameters used on 21 March 2022 were used on 18 May 2022. Two digesters were not operational (Figure 3), and therefore were not surveyed on 21 March 2022 and 18 May 2022. UAV operational and safety considerations identified on 18 May 2022 resulted in three additional digesters not being surveyed and another three digesters being surveyed in one direction (Figure 3).

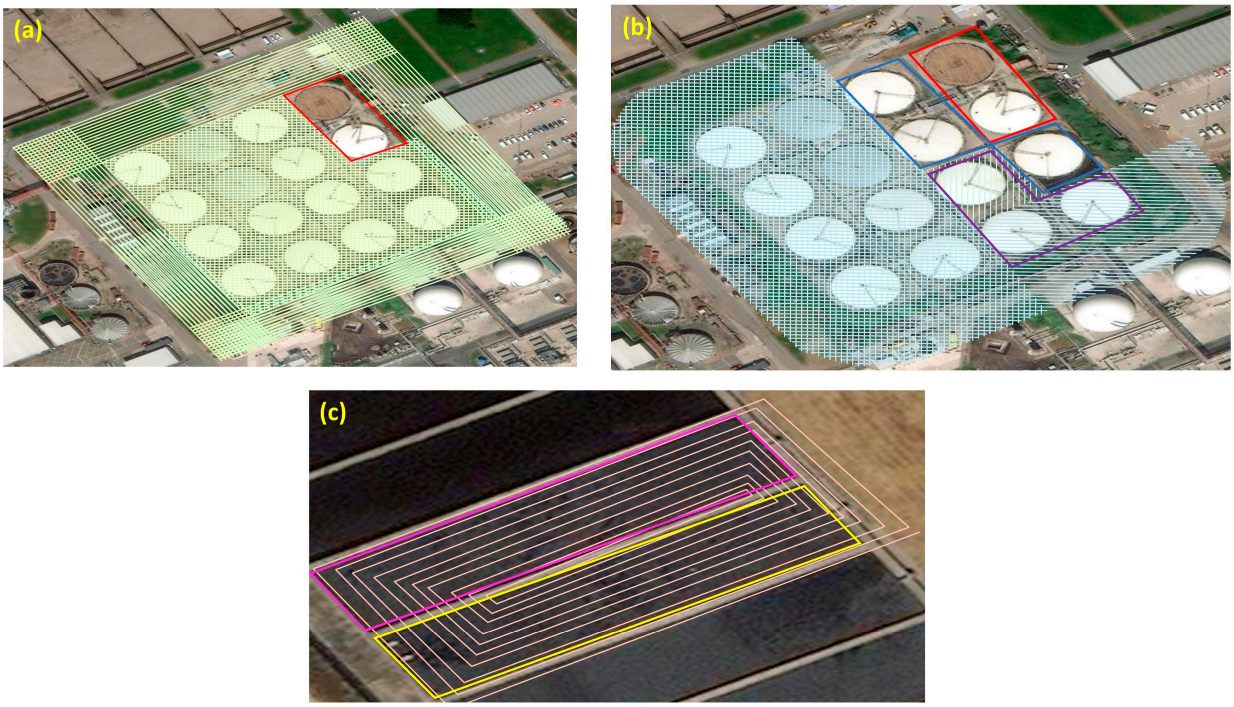

Figure 3. UAV flight plan designs for the anaerobic digesters (**a**,**b**) and the digestate storage tank (**c**): generated using ArcGIS Pro 2.8 (Esri, USA). Source: [17]. (**a**) 21 March 2022. (**b**) 18 May 2022. Red polygons indicate non-operational anaerobic digesters. Blue polygons show those digesters that were not surveyed on 18 May 2022. Purple polygons show those digesters that were surveyed only in one direction. Plate (**b**) shows the effect of the UAV operational and safety constrains on 18 May 2022. Plate (**c**) shows each bay surveyed in Pink and Yellow colour. Both bays combined constitute a tank.

The digestate storage tanks were surveyed on 4th November 2022. The first mission was an initial inspection flying across all tanks to identify the tank with the highest CH_4 emissions. A detailed survey of this tank was carried out in the second mission. The UAV was flown following a concentric rectangular flight path (20 min) (Figure 3). The flight altitude was maintained constant at 20 m from the take-off point. Vertical path integrated CH_4 concentrations were measured every 2 m with the U10 laser in nadir position. The total area surveyed was $\approx$1430 m^2. The data collection and data processing workflow are presented in Figure 4.

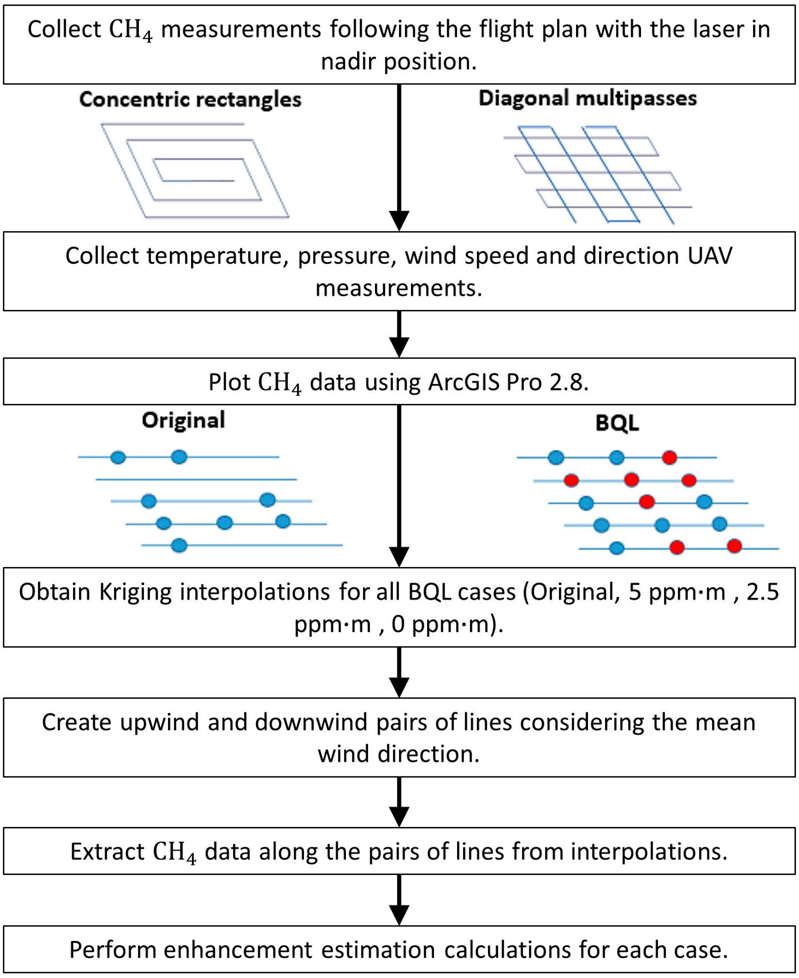

Figure 4. Workflow depicting the data collection and processing followed. BQL stands for below quantification level.

Three missions were required to survey the cake pads on 18 March 2022. The first mission was conducted at a flight altitude of 20 m. The second mission was undertaken at 2 m altitude with the sensor pointing to the ground. The final mission was conducted at 2 m of altitude with the sensor pointing parallel to the ground and aiming at the retention concrete structures defining the limits of each bay. The total flight time was 30 min and the area covered was approximately 1560 m^2.

2.3.2. Ancillary Data

Multiple ancillary data sets were collected (Table 2) and included: altitude, GPS location, wind speed and direction, temperature, pressure and angle of the U10 laser. The majority of variables were logged by sensors already embedded in the UAV platform. Technical details about the specific sensors used by DJI were not available from the manufacturer's manual or the technical support help lines, so further information cannot be reported. Other variables were manually noted for each flight based on information provided by the Matrice 300 RTK (DJI, Shenzhen, China) controller.

Data from a set of 12 ground-based metal oxide sensors (Baker Hughes, Houston, TX, USA) located at the perimeter of the cake pad (Figure 1) were also used to understand temporal and seasonal variations and to sense-check the measurements obtained with the U10 sensor. The metal oxide sensor (Baker Hughes, USA) quantifies CH_4 concentration using the solid-state sensor working principle [23]. In metal oxide sensors, the target gas is adsorbed on to a sensing layer which consists of metal oxides. When the target gas gets adsorbed to the sensing layer, the gas gets dissociated into ions or complexes and electrons.

These electrons get accumulated on the surface of the metal oxide resulting in conductivity or resistivity changes to the sensing layer. The sensor output voltage varies accordingly with respect to the sensing layer resistance. Therefore, the sensor output voltage is a measure of gas concentration [24]. The Baker Hughes' CH_4 sensor network was used in this study due to its ability to detect low concentration levels (2–1000 ppm at ±3% or 5 ppm) when compared to other commercially available metal oxide sensors such as the TGS2611 sensor (Figaro, Osaka, Japan) (500–10,000 ppm) [25]. Within the Baker Hughes' network, each node consisted of a weather station and solar panels. All sensors were calibrated by the manufacturer as and when required or scheduled. The ground sensors continuously monitored CH_4 concentrations every 4 s. Each of these 12 nodes also had sensors to record an additional set of parameters, including temperature, relative humidity, wind speed and direction. Details about the specific sensors used was not available from the Baker Hughes' technical manual so further details cannot be reported. The ground sensors rely on a base station that transmits the data collected to the cloud (Figure 1). A subset of ground sensor data from 18 March 2021 (16:16) to 30 March 2022 (23:59) from the 12 sensors was used to characterize temporal and seasonal CH_4 patterns within the zone. An additional subset of measurements recorded during the flight missions was used to assess temporal variability of CH_4 and wind patterns during the UAV missions conducted on 18 March 2022, 21 March 2022 (13:11–17:45), 18 May 2022 (10:27–15:57) and 4 November 2022 (13:30–13:42), and for UAV ancillary data sense-check purposes.

2.4. Data Analysis

2.4.1. Characterization of Prevailing Winds

For all the assets surveyed, the mean wind speed and direction derived from direct UAV measurements were considered as the prevailing wind characteristics during the survey. Data from the ground sensors were used to identify variations in wind conditions during the UAV surveys using wind roses. The ground sensor data were also used to sense-check the wind conditions derived from the UAV measurements. All calculations were carried out using the Openair package in R (R Core Team, Vienna, Austria).

2.4.2. Influence of Emissions from Adjacent Sources

Time series plots from 18 March 2021 to 30 March 2022 were obtained for those ground sensors which recorded highest and lowest CH_4 concentrations to ascertain how the influence of assets adjacent to the cake pad varies over time. The period of 18 March 2021 to 30 March 2022 was selected because it captured variations throughout the year.

Data from the ground sensors collected during each UAV survey were analysed using the pollution rose option within the Openair package in R (R Core Team, Austria) to identify possible sources of CH_4 linked to adjacent assets or close by features (e.g., M6 motorway and Kingsbury Road A4097). Pollution roses portray the proportion of pollutant concentration (CH_4) that is within a certain range of wind direction [26].

The U10 vertical path integrated CH_4 concentration data collected for the anaerobic digester buffer area was used to visually identify potential adjacent sources of CH_4 emissions, as well as path integrated background concentrations. The path integrated background concentrations were estimated through interpolation as described in Section 2.4.3.

2.4.3. Identification of CH_4 Sources

For the anaerobic digesters, U10 CH_4 measurements were interpolated using geostatistical methods (Kriging) in ArcGIS pro version 2.8 (Esri, USA) to generate a raster surface of predicted vertical path integrated CH_4 concentrations and prediction standard errors [13]. Prediction standard errors represent the uncertainty of the predicted values by the Kriging method. The cross-validation tool in ArcGIS Pro 2.8 (Esri, USA) was used to assess the mean standardized error of the applied semivariogram model. The interpolation was conducted three times to account for the uncertainty in measurements below quantification level (BQL), assuming all BQL measurements to be (i) 5 ppm·m, (ii) 2.5 ppm·m and (iii) 0 ppm·m.

Herein after, interpolations for each of these data sets are named BQL_5, BQL_2.5 and BQL_0. The interpolation with the raw values is named BQL_original. Data records were assumed to be distributed at 2 m intervals as per U10 default surveying specifications [15]. All missing records along the flight path were assumed to be BQL.

Kriged results were used to obtain upwind and downwind measurements of vertical path integrated CH_4 concentrations. For the anaerobic digesters, seven pairs of lines perpendicular to the mean wind direction were plotted upwind and downwind of each digester on the prediction surface (Figure 5). Line lengths varied from 26 m to 32 m as they extended from both sides concentrically. Pairs of lines were limited to seven to ensure no overlapping with adjacent assets occurred. A total of 1000 equally spaced points were created along each line, resulting in a maximum distance of 3.2 cm between two consecutive points. CH_4 measurements and prediction standard errors along the lines were extracted from the equally spaced points (every 2.8 cm to 3.2 cm) using ArcGIS Pro version 2.8 (Esri, USA). The number of points per line was set to 1000 to provide sufficient input data to calculate CH_4 enhancement using Equation (1) under the assumption of stable wind conditions for open-path TDLAS [9], while balancing the computational time. Path integrated background concentrations were represented by path integrated upwind concentrations. To account for the effect of path integrated background concentrations, upwind measurements were averaged per line and mean upwind measurements were deducted from each measurement of the corresponding downwind line. The resulting values were summed together to estimate the CH_4 enhancement associated with each parallel pairs of lines [9,18] and averaged to identify whether a specific digester was acting as a CH_4 source (i.e., digesters resulting in positive enhancement values). These enhancements (ppm·m^2) were obtained assuming that the emissions were continuous throughout the data collection period, the wind speed was stable and CH_4 flowing in to and out from the specific volume considered would occur through the upwind and downwind surfaces only (Equation (1)).

$$\text{Enhancement} = \int ([CH_4]_i - [CH_4]_b)dx \tag{1}$$

where $[CH_4]_i$ is the ith downwind CH_4 measurement along the line (ppm·m), $[CH_4]_b$ is the background CH_4 measurement which is measured upwind of the source (ppm·m) and dx is the infinitesimal difference along horizontal direction in the plane perpendicular to the wind speed (m).

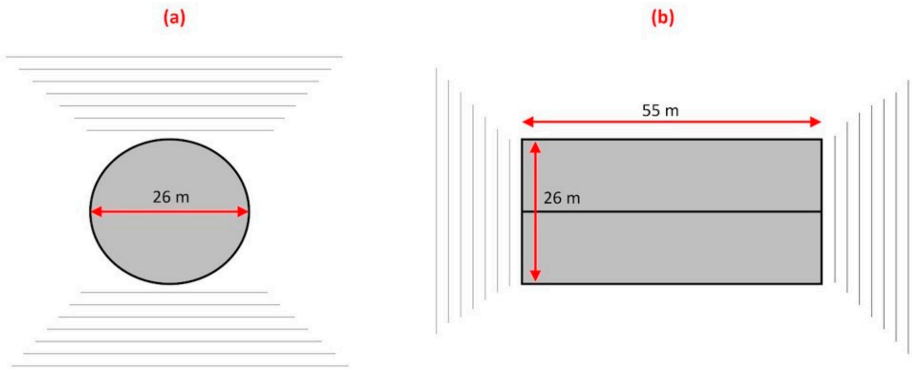

Figure 5. Demonstration of the lines (red) used to determine upwind and downwind measurements for the anaerobic digesters (**a**) and digestate storage tanks (**b**). Source: [17].

For the digestate storage tanks, upwind and downwind measurements were extracted from tank 8 (Figures 1 and 5). Upwind and downwind pairs of lines were also created, with lengths varying from 26 m to 32 m and each having 1000 points. Data extraction, path integrated background concentration and enhancement estimation were carried out as per the anaerobic digesters.

For the cake pads, the differences between ground sensor measurements recorded upwind and downwind of the cake pads were observed to qualitatively identify whether adjacent assets and cake pad were acting as sources.

3. Results

3.1. UAV and Ancillary Data

Mean values of relative humidity, temperature, pressure, wind speed and direction for the flight duration derived from the UAV platform for each survey date are summarized in Table 2. The total number of CH_4 measurements above quantification level obtained for the anaerobic digestors were 3989 on 21 March 2022, reduced to 3771 after excluding isolated measurements, and 284 on 18 May 2022. Winds were predominantly southeasterly (21 March 2022) and southerly (18 May 2022) (Table 2). Based on the UAV wind records (Table 2), the wind speed doubled on 18 May 2022 when compared to 21 March 2022. There were slight differences in temperature and pressure. The relative humidity was approximately the same during both days. Only a few measurements were recorded on top of the six digesters located in the north westbound (digesters number 9 to 15 in Figure 6, see also Figure 1) during the survey conducted on 21 March 2022. These isolated measurements were excluded from the analysis as these would not have enabled enhancement estimation. The number of measurements above BQL was 14 times larger than on 18 May 2022 (Table 2).

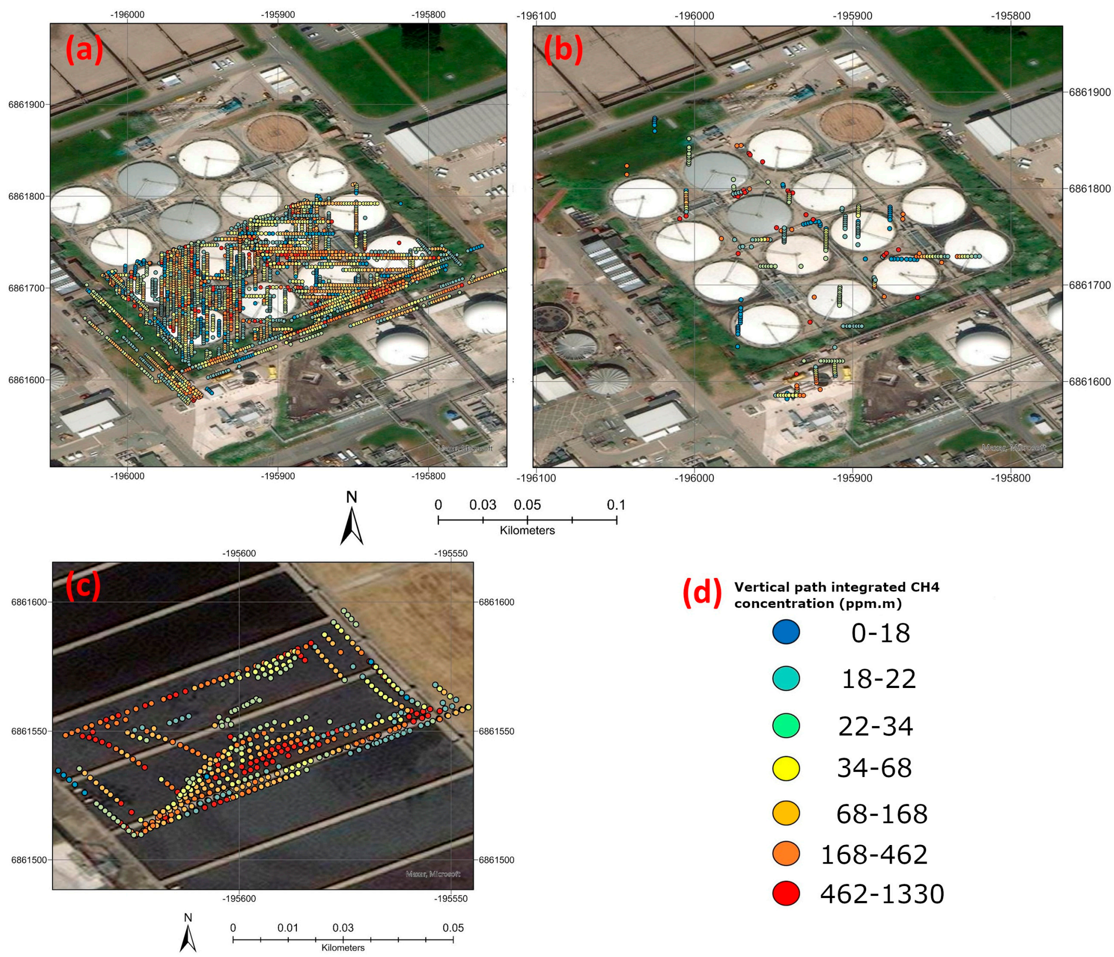

Figure 6. Raw CH_4 measurements registered above the quantification level for the anaerobic digesters (**a**,**b**) and the digestate storage tank (**c**), generated using ArcGIS Pro 2.8 (Esri, USA). Source: [17]. (**a**) 21 March 2022. (**b**) 18 May 2022. (**c**) 4 November 2022. (**d**) Vertical path integrated CH_4 concentration colour scale in ppm·m. These represent the spatial distribution of vertical column integrated CH_4 concentrations in ppm·m.

For the digestate storage tanks, the number and magnitude of CH_4 measurements registered was largest for tank 8 (Figures 1 and 6). A total of 532 CH_4 measurements above the quantification level were detected (4 November 2022) for tank 8. Based on the UAV data, the direction of the wind was northwesterly during the survey (Table 2).

For the cake pad, no CH_4 readings above the quantification level could be detected at 20 m or 2 m altitude when using the sensor in nadir position. Treating those readings as either 0 ppm·m, 2.5 ppm·m or 5 ppm·m would have resulted in a homogeneous layer of vertical path integrated CH_4 concentration above the cake pads, and therefore no enhancement values could be estimated. The low reflectance power of the cake pad required for the UAV platform to fly 2 m above the cake and the U10 sensor to be pointed towards the walls defining the structural perimeter to record path integrated CH_4 concentrations. Unfortunately, these records did not provide information about concentration within the vertical column at a given point and could not be analysed further.

3.2. Characterisation of Prevailing Winds

A total of 2078 measurements per ancillary variable were obtained from the ground sensors for the 21 March 2022 during the anaerobic digester survey. On 18 May 2022, 3029 measurements per variable were recorded. The prevailing wind conditions were not consistent with those reported by the UAV (Table 2). However, the maximum wind speed recorded by the ground sensors was 3.21 m s^{-1} on 21 March and 5.81 m s^{-1} on 18 May 2022, values that were very similar to those reported by the Matrice 300 RTK wind sensors. The wind rose showed that southeasterly winds were more prominent during the survey conducted on 21 March 2022. Approximately 15% of the total measurements were the same as the range of mean wind direction derived from the UAV ($151° \pm 9°$). On 18 May 2022, southeasterly and southerly winds were more dominating and approximately 10% of the total measurements were the same as the range of mean wind direction derived from the UAV ($194° \pm 5°$). Overall, results indicated that the wind conditions could be considered more stable for the anaerobic digesters during the survey conducted on 21 March 2022 when compared to the survey on 18 May 2022.

During the digestate storage tanks survey (4 November 2022) a total of 183 wind measurements were recorded for each ground sensor. The mean or maximum wind speed was not consistent with those reported by the UAV sensors (Table 2). On 4 November 2022, northwesterly winds were more prominent during the mission. Approximately 18% of the total measurements were same as the mean wind direction reported by the UAV (302°).

During the cake pad survey, on 18 March 2022, a total of 428 measurements per ancillary variable were recorded during the flight period per ground sensor. There were southeasterly winds with the highest wind speed reaching 2.10 m s^{-1}. Wind speed and direction values could not be compared to the UAV measurements as no UAV records were obtained. The wind roses obtained for 18 March 2022 showed that southeasterly winds were more prominent.

These differences in wind measurements showcase differences in surveying conditions at ground and flight heights, in addition to differences in sensor recording methods and frequencies.

3.3. Influence of Emissions from Adjacent Sources

For the cake pad, the time series plots for CH_4 concentration were obtained for the one-year pre-survey period for six of the twelve ground sensors which recorded highest and lowest CH_4 measurements (Figure 7). Sensors 2, 3 and 12 showed the highest variation patterns and concentration levels. They were located at the north and northwest perimeter (Figure 1), which was further away from the landfill and in close proximity to other assets (e.g., digesters, centrifuges, gravity thickeners) with maximum values of mean monthly and hourly (Monday and Wednesday) CH_4 concentrations >14 ppm. All three showed similar hourly patterns and a negative trend in daily variation.

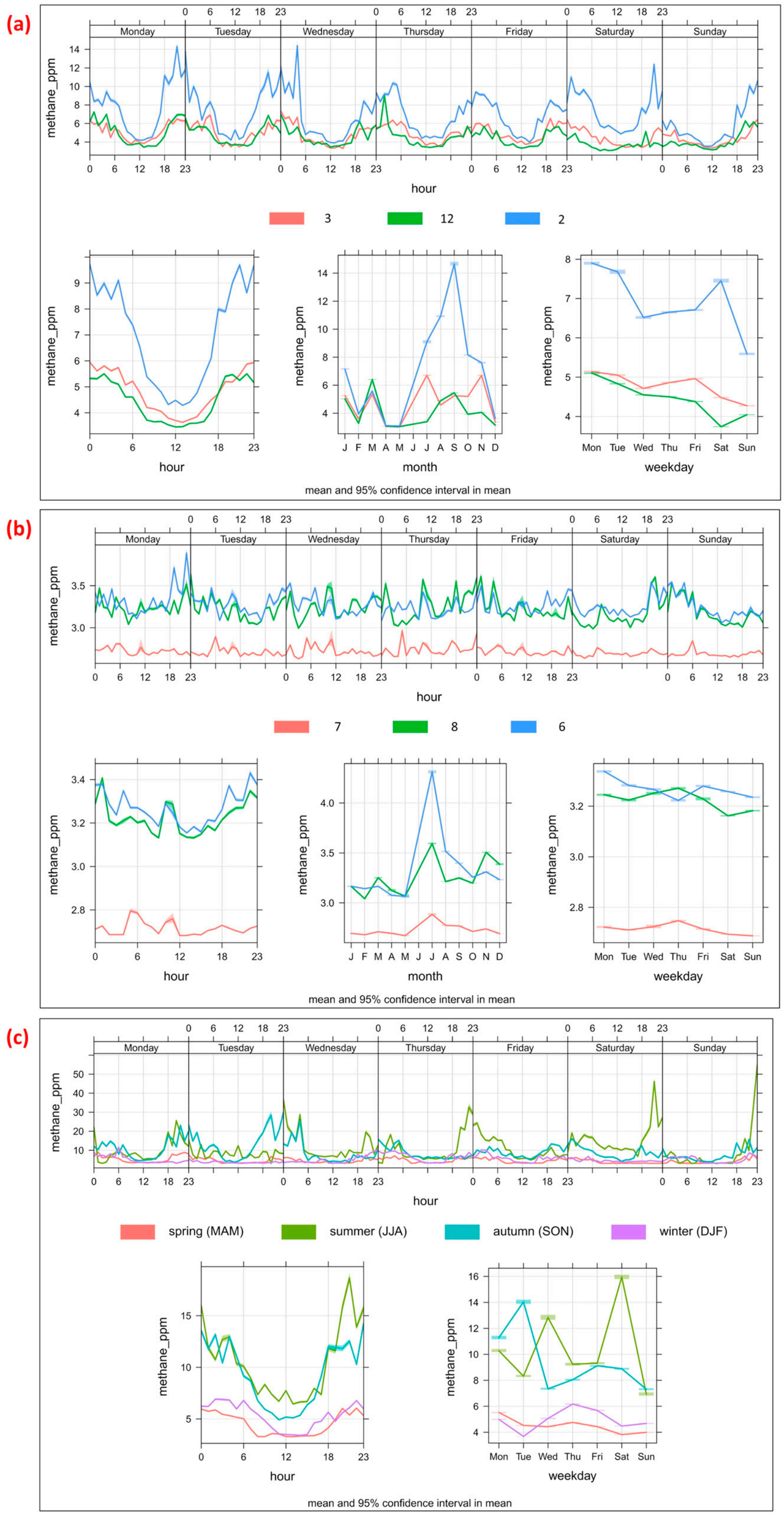

Figure 7. Time series plots for the ground sensors (**a**) 2, 3 and 12, (**b**) 6, 7 and 8 and (**c**) seasonal variation located around the cake pad: generated using Openair package, R (R Core Team, Austria). Data used corresponds to the one-year pre-survey period from 18 March 2021 to 30 March 2022. CH_4 is given in ppm and the shaded area represent the 95% confidence interval in mean. MAM, JJA, SON and DJF stand for March–April–May, June–July–August, September–October–November and December–January–February, respectively. The location of each sensor is depicted in Figure 1.

Sensors labelled 6, 7 and 8, which were located at the east perimeter (Figure 1), close to the landfill and comparatively isolated from other assets, were relatively more stable and no specific pattern could be seen other than the fluctuations (Figure 7). However, there was a slight negative trend towards the weekend in daily variations. Values of mean hourly, daily and monthly CH_4 concentration did not exceed 5 ppm. Seasonal variations for sensor 2, which recorded the highest CH_4 concentrations, were highest during summer and lowest during spring (Figure 7).

The pollution roses for the ground sensor data collected on the 18 March 2022 (Figure 8) showed that the landfill and the motorway M6 did not have an effect on the CH_4 concentrations recorded for the cake pad. Both landfill and M6 were located to the east from the cake pad. However, the ground sensors (1, 2, 9, 10, 11, 12) located west of the cake pad and further away from the landfill showed higher frequencies for concentration levels >9 ppm, which is the lower end of the top concentration interval recorded that day (Figures 1 and 8). The ground sensors (4, 5, 6, 7, 8) which were located to the east of the cake pad and closer to the landfill showed lower frequency for CH_4 concentrations >9 ppm, with the majority of values being between 0 ppm to 4 ppm. As the sensor gets closer to the landfill, the frequency of high concentration readings decreased. For example, when looking at sensor 3, the majority of the concentration levels were between 2 ppm and 4 ppm, with approximately 3% of the measurements were >9 ppm. Instead, sensor 7, which was the closest to the landfill, showed concentrations of only up to 4 ppm and the majority of them were between 2 ppm to 3 ppm. Overall, sensors located downwind of the cake pads showed higher concentrations to those located upwind when easterly winds were present; this showing that there is no evidence of landfill CH_4 emission influencing CH_4 measurements during this period for this asset.

Southeasterly winds were most prominent on 21 March 2022. Sensors located upwind of the cake pad (5, 6, 7, 8, 9, 10, 11) recorded lower concentrations < 6 ppm compared to others, and the majority of the measurements were between 2 ppm to 4 ppm. Ground sensors which were located downwind of the cake pad (1, 2, 3, 4, 12) showed higher concentrations > 16 ppm.

The pollution roses for the survey conducted on the 18 May 2022 showed that the frequency for concentrations > 7 ppm, the minimum level of the highest concentration range recorded (Figures 1 and 9), was higher when the wind was flowing from west and southwest. West and southwest winds define the direction where the digestate storage tanks, anaerobic digesters, gas bags and other adjacent assets in close proximity are located. Sensors (2, 3) which were located downwind of the cake pad recorded concentration > 7 ppm when there were southerly and southeasterly winds as well. A similar pattern was observed for sensor 10, although this sensor was located upwind of the cake pad. Sensors (4, 5, 7) which were located further away from the adjacent assets reported lower concentrations in comparison to other sensors. Sensor 7, which was the furthest from the adjacent assets and closest to the landfill, reported the lowest concentrations among all, with the majority of records between 2 ppm and 3 ppm and a maximum of 4 ppm.

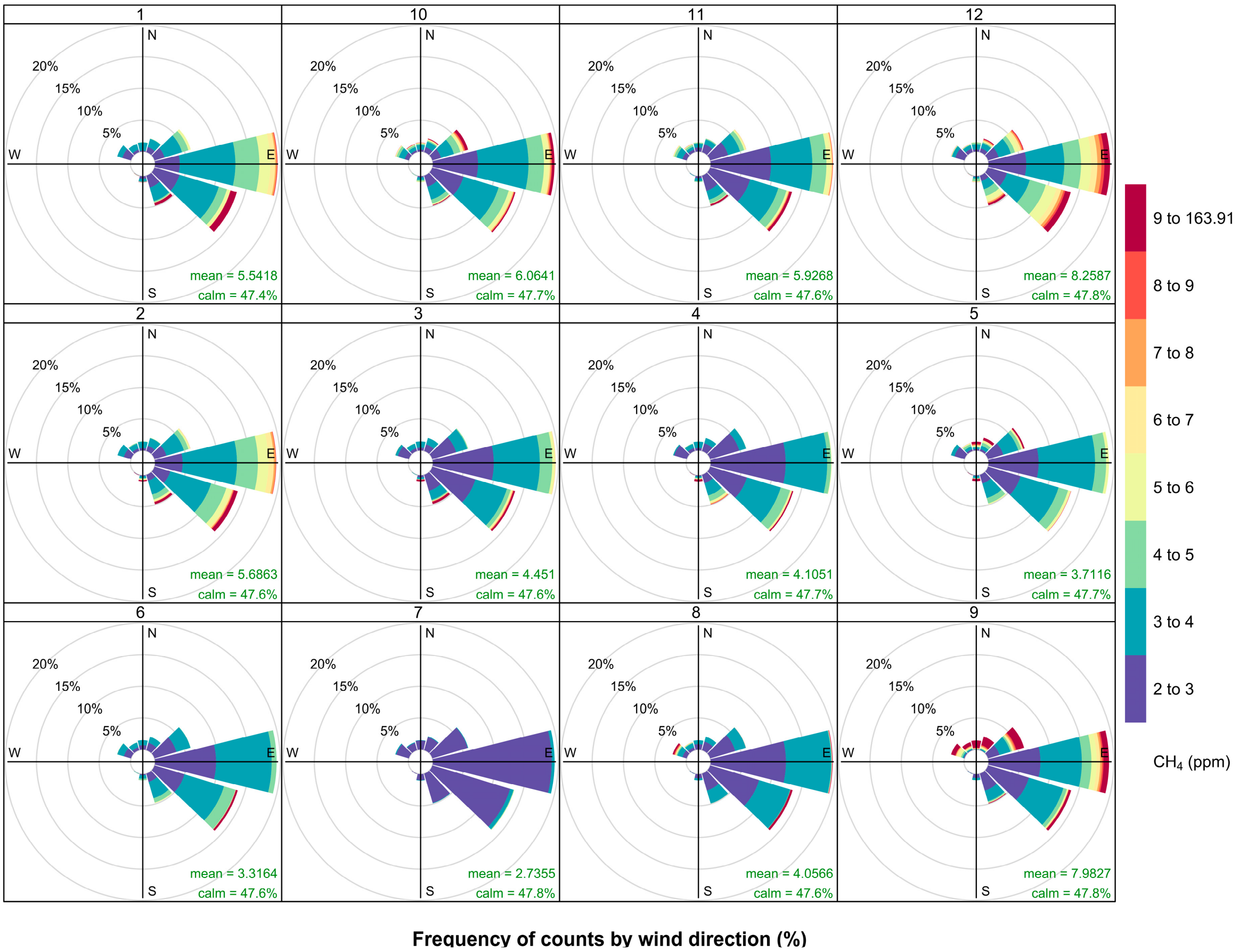

Figure 8. Pollution rose for each metal oxide semiconductor sensor on (18 March 2022): generated using Open-air Package, R (R Core Team, Austria). Colour and grey circles represent the concentration level in ppm and the percentage of CH_4 measurements within a certain range of wind direction, respectively. For each sensor, the mean CH_4 concentration is given in ppm. Calm represents the percentage where the recorded wind speeds were 0 m s^{-1} for each sensor. Wind directions are in Met Office format. CH_4 concentrations are plotted against the wind direction; therefore, these do not represent concentration levels when wind speed was 0 m s^{-1}. The sensor label is displayed on top of each graph (e.g., 1, 2, 3).

For the anaerobic digesters on 21 March 2022, the fitted semivariogram models for BQL_original, BQL_5, BQL_2.5 and BQL_0 were exponential, spherical, circular and circular, respectively. On 18 May, the semivariogram models were spherical and exponential for BQL_original and other BQL cases, respectively. When looking at the buffer area interpolations (Figure 10) for 21 March 2022, most of the area near the gas bags, which was upwind of the source, presented high vertical path integrated concentrations (170–365 ppm·m (red), 76–170 ppm·m (orange) or 64–76 ppm·m (yellow)) for all BQL cases. The proportion of these colours was smaller in BQL cases than for the original case (Figure 10). These results indicated that the gas bags could be acting as possible external CH_4 sources.

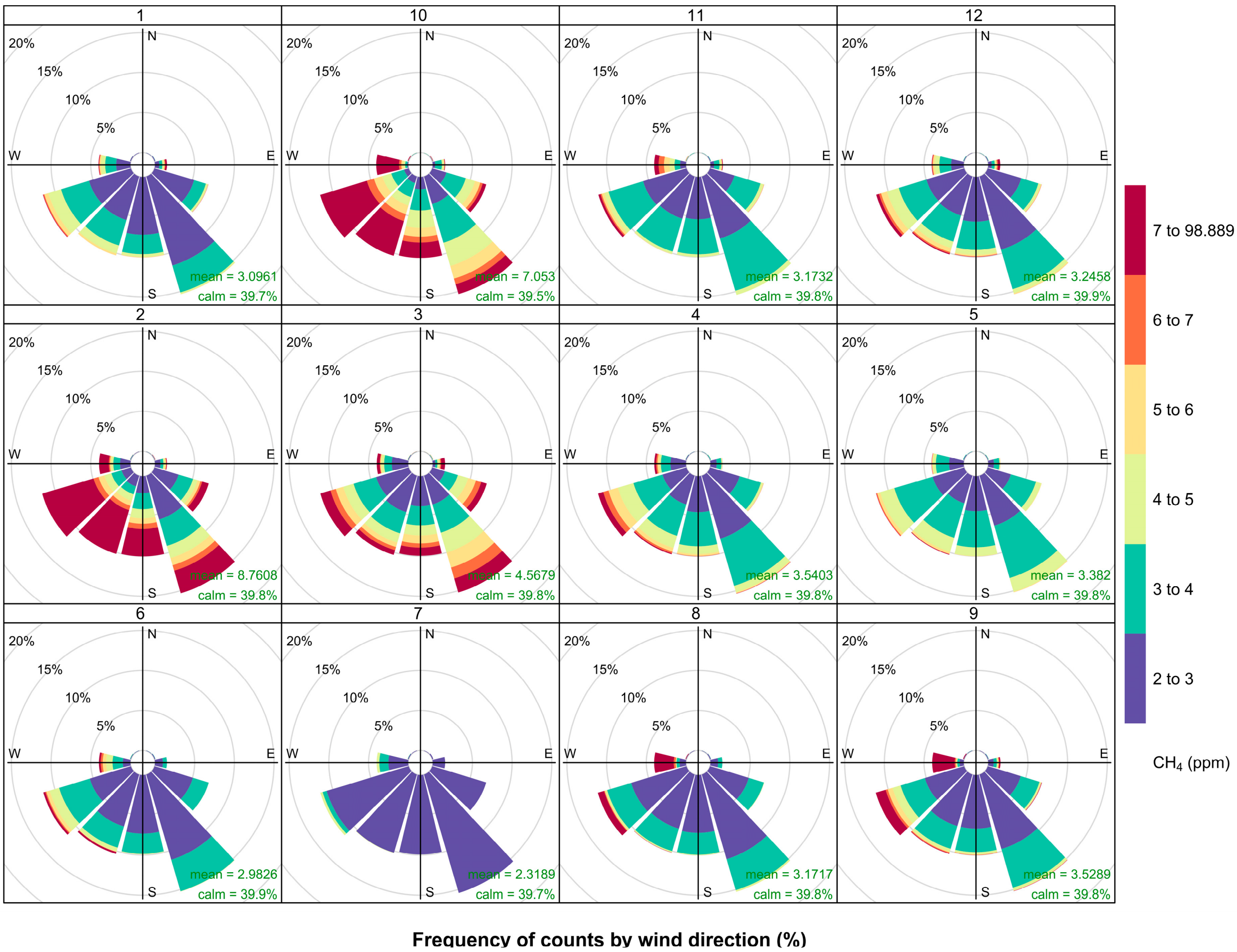

Figure 9. Pollution rose for each metal oxide semiconductor sensor (18 May 2022): generated using Open-air Package, R (R Core Team, Austria). Colour and grey circles represent the concentration level in ppm and the percentage of CH_4 measurements within a certain range of wind direction, respectively. For each sensor, the mean CH_4 concentration is given in ppm. Calm represents the percentage where the recorded wind speeds were 0 m s^{-1} for each sensor. Wind directions are in Met Office format. CH_4 concentrations are plotted against the wind direction; therefore, these do not represent concentration levels when wind speed was 0 m s^{-1}. The sensor label is displayed on top of each graph (e.g., 1, 2, 3).

Interpolations for 18 May 2022 (Figure 11) did not highlight any external source due to the lower number of measurements recorded resulting in a more homogeneous surface.

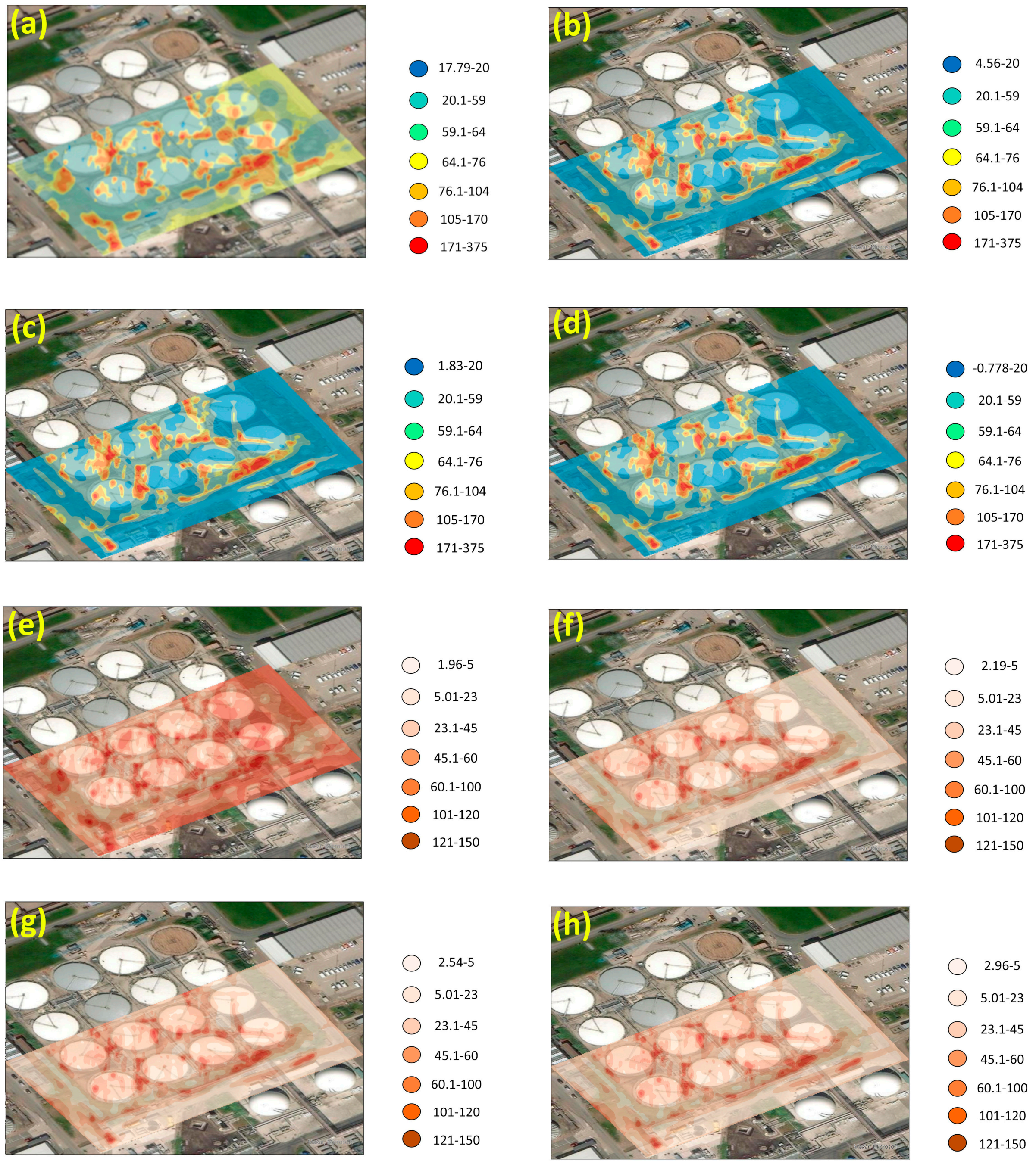

Figure 10. Kriging interpolations and prediction standard error surfaces of vertical path integrated CH_4 concentrations (21 March 2022) for the anaerobic digesters: generated using ArcGIS Pro 2.8. Source: (Esri, 2023). Kriging interpolations: (**a**) Original data set. U10 CH_4 measurements below the detection level were set to (**b**) 5 ppm·m, (**c**) 2.5 ppm·m and (**d**) 0 ppm·m. Prediction standard error surface: (**e**) Original data set. U10 CH_4 measurements below the detection level were set to (**f**) 5 ppm·m, (**g**) 2.5 ppm·m and (**h**) 0 ppm·m.

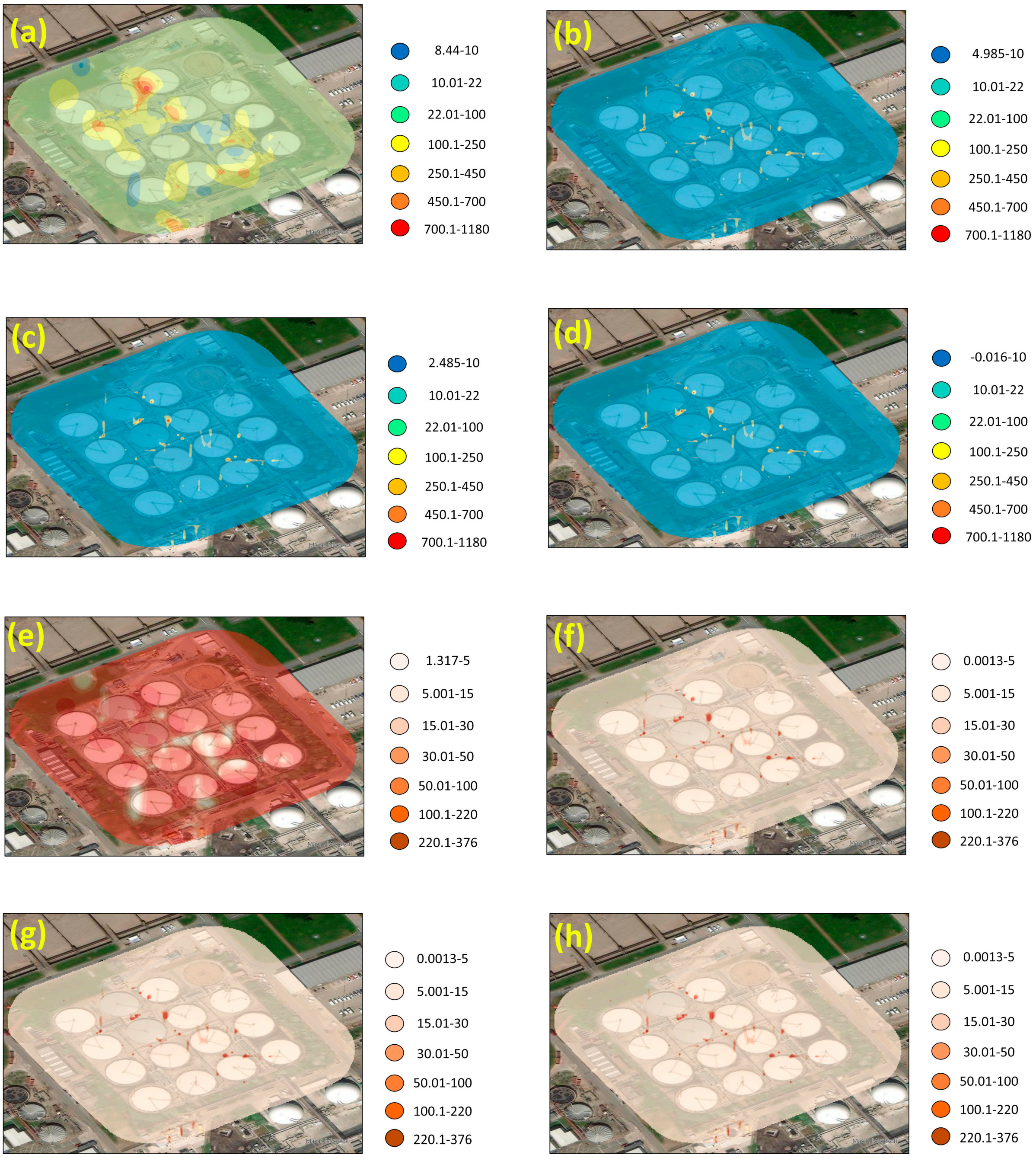

Figure 11. Kriging interpolations and prediction standard error surfaces of vertical path integrated CH_4 concentrations (18 May 2022) for the anaerobic digesters: generated using ArcGIS Pro 2.8. Source: (Esri, 2023). Kriging interpolations: (**a**) Original data set. U10 CH_4 measurements below the detection level were set to (**b**) 5 ppm·m, (**c**) 2.5 ppm·m and (**d**) 0 ppm·m. Prediction standard error surface: (**e**) Original data set. U10 CH_4 measurements below the detection level were set to (**f**) 5 ppm·m, (**g**) 2.5 ppm·m and (**h**) 0 ppm·m.

The semivariogram models fitted for the data collected on 4 November 2022 for BQL_original, BQL_5, BQL_2.5 and BQL_0 were always exponential, except for BQL_2.5 which was circular. In digestate storage tanks, the buffer area interpolations (Figure 12) did not provide information on external sources. However, higher vertical path integrated concentration levels (Red: 320–615 ppm·m, Orange: 150–320 ppm·m) could be observed downwind to tank 8 for all BQL interpolations (Figure 12). This indicated that emissions for tank 8 were higher than any of the tanks located further upwind (tank 6 and 7).

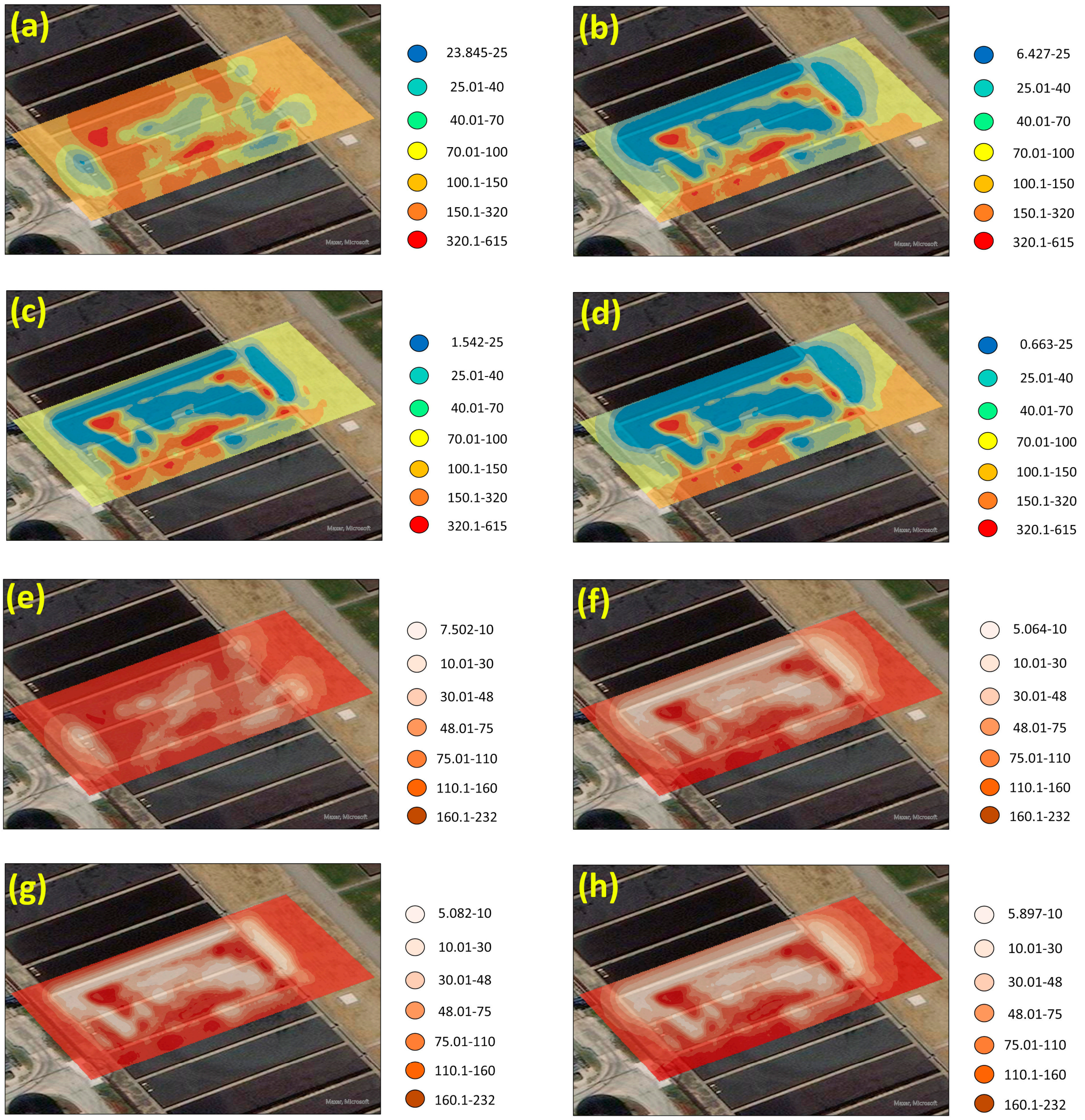

Figure 12. Kriging interpolations and prediction standard error surfaces of vertical path integrated CH_4 concentrations (4 November 2022) for the digestate storage tanks: generated using ArcGIS Pro 2.8. Source: (Esri, 2023). Kriging interpolations: (**a**) Original data set. U10 CH_4 measurements below the detection level were set to (**b**) 5 ppm·m, (**c**) 2.5 ppm·m and (**d**) 0 ppm·m. Prediction standard error surface: (**e**) Original data set. U10 CH_4 measurements below the detection level were set to (**f**) 5 ppm·m, (**g**) 2.5 ppm·m and (**h**) 0 ppm·m.

3.4. Identifying CH_4 Sources

For the anaerobic digesters, enhancement estimations obtained for BQL_2.5 and BQL_0 did not present differences to those obtained for BQL_5. Therefore, only results obtained for BQL_original and BQL_5 were compared.

On 21 March 2022, digesters 1, 2, 5 and 8 (Figure 13) had positive enhancements for both BQL_original and BQL_5 and therefore could be considered as potential sources. Digesters 3, 4 and 7 had no positive enhancements for both BQL_original and BQL_5. Results for digester 6 were variable (source to no-source) depending on whether the BQL data were processed (BQL_5, BQL_2.5, BQL_0) or not (BQL_original); only BQL_original resulted in a positive enhancement. BQL_original reported the highest enhancement for digester 2 (327 ppm·m^2) while it was lowest for digester 8 (14 ppm·m^2). BQL_5 reported the highest enhancement estimation for digester 1 (769 ppm·m^2) and the lowest for digester 5 (44 ppm·m^2).

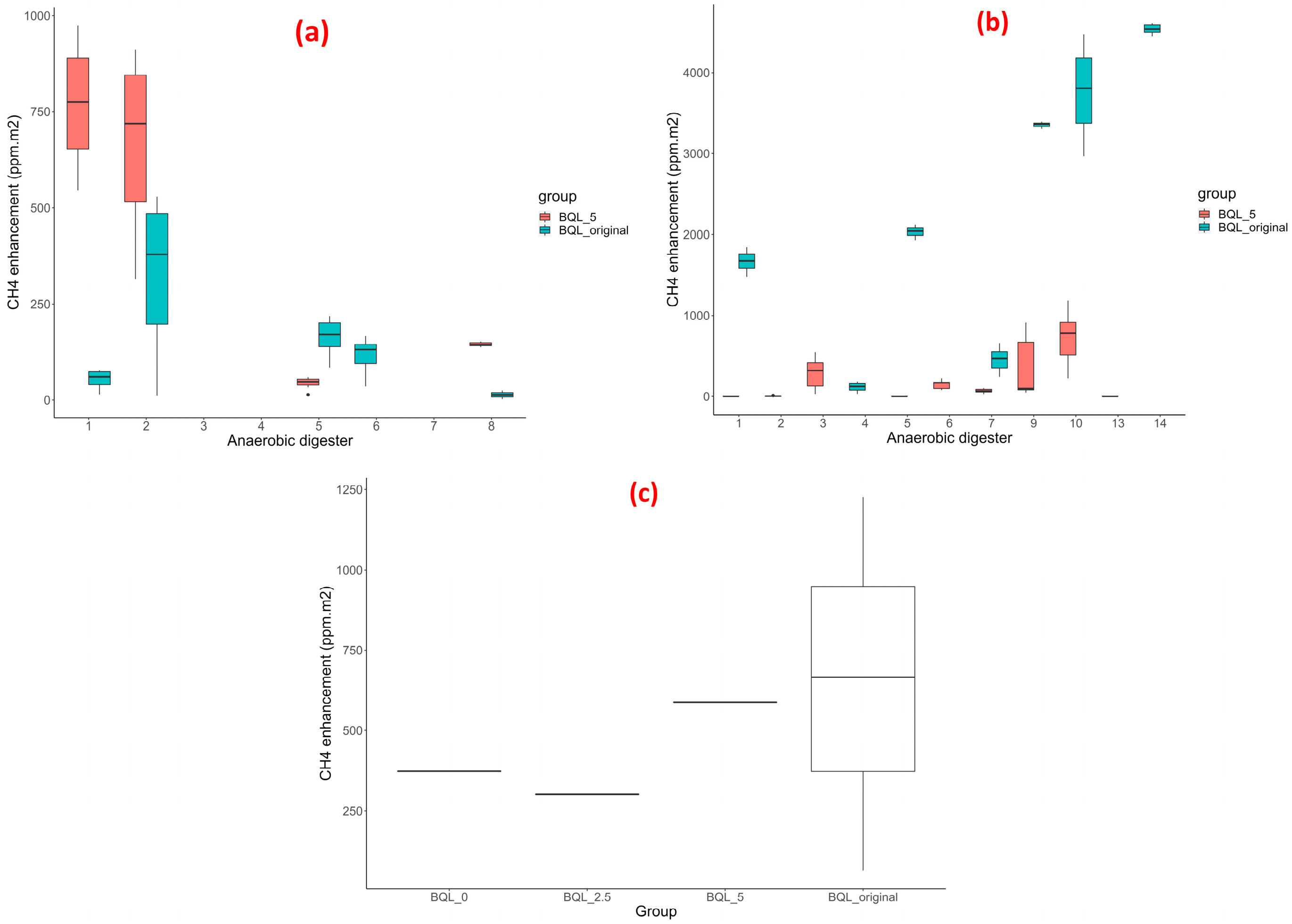

Figure 13. CH_4 enhancement estimations for each anaerobic digester (**a**,**b**) and the digestate storage tank (**c**). The boxes represent the inter quartile range. BQL_5, BQL_2.5 and BQL_0 represent the enhancement obtained when considering all values below quantification level to be 5 ppm·m, 2.5 ppm·m and 0 ppm·m, respectively. For BQL_original, enhancement was calculated with the raw data. (**a**) 21 March 2022 (**b**) 18 May 2022 and (**c**) 4 November 2022.

On 18 May 2022, digesters 1, 5, 7, 9 and 10 had positive enhancements for BQL_original and BQL_5. For the other digesters, positive or negative enhancements were obtained depending on whether the BQL data were processed (BQL_5, BQL_2.5, BQL_0) or not (BQL_original) (Figure 13). BQL_original reported the highest enhancement estimation for digester 14 (4538 ppm·m^2) and the lowest for digester 4 (116 ppm·m^2). BQL_5 reported the highest enhancement estimation for digester 10 (720 ppm·m^2) and the lowest for digester 1 (0.003 ppm·m^2).

For digestate storage tanks, differences in enhancement estimation were observed between BQL_original, BQL_0, BQL_2.5 and BQL_5 (Figure 13). The tank had positive enhancements independently on how BQL values were treated. BQL_original reported the highest enhancement estimation (656 ppm·m^2) whereas BQL_2.5 reported the lowest (300 ppm·m^2).

4. Discussion

This paper presents a novel UAV-U10 approach to quantify vertical path integrated CH_4 concentrations from selected WWTP assets. The aim was to develop a set of UAV-U10 data collection strategies for open and closed WWT assets. A conceptual diagram summarizing the framework and the key findings and recommendations around data collection strategies is presented in Figure 14.

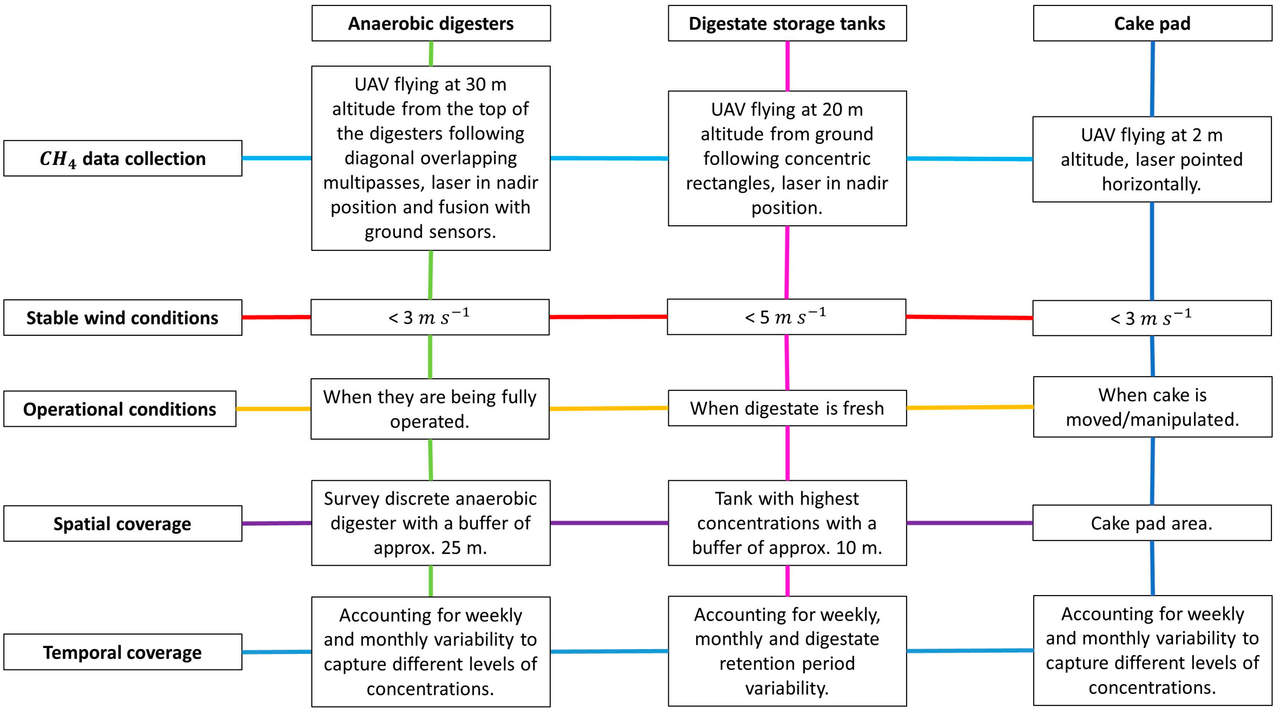

Figure 14. Diagram summarizing recommended data collection strategies based on the U10-UAV sensor thresholds, methodological limitations and results from the ground sensor temporal analysis.

The framework requires the estimation of background concentrations for CH_4 enhancement quantification. Previous studies [27] used downwind out-of-plume measurements as the background concentration. This approach would only be suitable when such measurements are actually out-of-plume and no other external sources are nearby. The distribution of assets at Minworth WWTP is quite dense, with all the assets situated in close proximity to each other. Adjacent assets are expected to have an influence on CH_4 enhancements and therefore the approach described by Allen et al. [27] is not valid for the study area. The approach of Allen et al. [27] treats the sampled sources independently and separately and does not take into account potential overlaps of adjacent plumes. This could result in double counting of plumes if they pass over multiple sources. The analysis of both upwind and downwind measurements for a given asset was thought to be more helpful in determining background concentrations and assessing whether CH_4 enhancement was caused by that specific asset or not. This required collection of CH_4 measurements around a buffer area (≈25 m wide for anaerobic digesters and ≈10 m wide for digestate storage tank). The width of the buffer was determined based on their proximity to adjacent assets and the U10 sensing capability.

The survey for some assets required in excess of 5 h to complete. Within this time frame, CH_4 plumes cannot be expected to be stationary. This limitation could curtail the future use of the UAV-U10 framework for flux estimation. An approach to overcome this challenge would be to conduct the survey in smaller discrete units for each asset. For example, the survey of the anaerobic digesters could be conducted for one digester at a time, at 20 min to 35 min per digester. Similarly, the digestate storage tanks could be surveyed one tank at a time. This will require for the interpolation to be conducted at tank or digester level. However, emissions from one anaerobic digester could influence the measurements of the adjacent anaerobic digester as they are separated by few meters leading to inability to distinguish where the actual emission is coming from.

Following the data collection strategy at Minworth, the use of overlapping multipasses is recommended to minimize the effect of temporal variation. For example, the anaerobic digesters were surveyed in two different directions (diagonal transects), which enabled estimation of an averaged CH_4 value for overlapping (replicate) points when interpolating.

Temporal variation occurs at different scales and not only during the duration of the UAV survey. This needs to be taken into account when defining the temporal frequency and spatial configuration of the UAV-U10 monitoring strategy in order to capture emission dynamics. Relative humidity levels were higher during nighttime in comparison to daytime, as recorded by the ground sensors. Similarly, CH_4 emissions were higher during nighttime compared to daytime for the cake pads. According to [28], CH_4 production increases with relative humidity in waste compost, as more pores in the compost appear and anaerobic conditions develop. This could explain the increment in CH_4 concentration of sludge cake. Biological degradation in composting is done under aerobic conditions, therefore, it is a contrasting process to sludge cake production. However, post processing of anaerobically digested sludge such as mechanical dewatering can lead to higher O_2 exposure [29]. Day to night wind speed variations could have influenced the concentration measurements from the ground sensors, as wind speed was lower during nighttime compared to daytime. When wind speed is high (>3 m s^{-1}), CH_4 tends to disperse faster, making it more difficult for the sensor to detect emissions. Aldhafeeri et al. [30] already mentioned that the sensing ability of solid-state sensors can be affected by wind speed and this effect has not yet been examined and understood to the full extent. Wang et al. [31] mentioned that humidity and temperature also could influence the sensitivity of the sensing layer in solid state sensors. The ground sensors are based on the solid-state principle, and therefore this could also explain the results obtained. Unlike the open systems, closed systems such as anaerobic digesters would not be expected to follow these daily patterns. However, there were no ground sensors located in close proximity to the anaerobic digesters to distinguish differences in temporal variability of CH_4 emission between open and closed systems.

There is also a need to consider within-a-week, as well as monthly CH_4 variations. CH_4 concentrations were highest on Mondays and decreased towards the end of the week, with the lowest point identified over the weekend. Mean monthly emissions are higher for those months where the cake pad is full or when the cake pad is moved out. Duan et al. [32] stated that livestock slurry forms a crust which traps produced CH_4 and mitigates CH_4 transport to the atmosphere, and trapped CH_4 gets oxidized by methanotrophic bacteria present in the crust in livestock slurry. Piled up cake also forms a crust; therefore, a similar phenomenon can occur in sludge cake as well, and when the crust is perturbed during the reallocation process a sudden release of remaining CH_4 could occur. However, these relations need to be further investigated. There were also differences in CH_4 concentration levels for different seasons (Figure 7) which could be caused by several environmental factors. Further research is required to better understand this effect. It is therefore recommended to support the UAV-U10 framework with ground-sensor information whenever possible. Further research should focus on the development of data fusion strategies and algorithms that enable the integration of data from multiple sources.

The survey strategy should be repeated at a frequency that captures weekly and monthly variations as the analysis of ground sensor data showed that CH_4 concentrations are lower during weekends, highest on Mondays and it differs from season to season. When it comes to spatial coverage, the flight plan should be designed to collect as much data as possible, maximizing spatial coverage. The monitoring framework presented here will not be able to capture temporal variability of emissions within a day as each mission takes 4.5 to 5.5 h.

Objective 2 looked at identifying those assets that could constitute potential emission sources. From the three assets surveyed, anaerobic digesters and digestate storage tanks could be identified as potential sources. However, it is not possible to compare enhancement estimation values to assess the source with the highest emission at this stage without converting these to fluxes. This is because weather conditions (temperature, pressure, wind speed and direction) were different between the two surveys and cannot be compared at enhancement level.

Results showed that CH_4 concentrations from the cake pads are more significant than the background emissions from the nearby landfill reaching the cake pads, as most of the higher concentration levels were detected by the sensors downwind of the cake pads (Figures 1 and 8). Therefore, at Minworth WWTP, the influence of the emissions from these external sources can be considered negligible for the measured CH_4 concentrations. Concentration levels went up on 18 May 2022, when there were westerly and southwesterly winds (Figure 9). There were many assets located west from the cake pad in close proximity such as anaerobic digesters, digestate storage tanks, gas bags, the centrifuge and the thermal hydrolysis plant. Therefore, it is possible for the measurements recorded to be affected by the emissions of these assets when the wind was from that direction.

CH_4 emissions from anaerobic digesters were detected with the U10 in nadir position and the UAV platform flying under stable wind conditions (<2.8 m s^{-1}), through diagonal multipasses spaced 2 m from each other and at 30 m of altitude from the top of the digesters (40–50 m from ground), where the lower bound is defined by safety operational restrictions, and the upper bound by the U10 capabilities. In turn, this limits the sensor ability to characterize the totality of any 3D plume. A significant reduction in the number of measurements recorded was observed on 18 May 2022. This could be due to CH_4 concentrations being low or to environmental factors, such as wind speed, affecting the sensitivity of detection of the U10. Note that wind speed doubled during the survey carried out on 18 May 2022 compared to the prevailing wind on 21 March 2022.

Ideal measurement conditions for digestate storage tanks, when following concentric rectangles, were a flight altitude of 20 m from take-off point, with the laser in nadir position and during stable wind conditions (<4.9 m s^{-1}). The highest CH_4 measurements were detected over the tank that contained fresher digestate (more semi-solid consistency rather than crust). CH_4 emission from digestate storage tanks is dynamic as the potential of the digestate to emit CH_4 varies based on the freshness of the digestate. Fresh digestate is expected to have higher levels of dissolved CH_4 and it is expected to be released over time due to residual methanogenic activities. In addition, higher temperature levels in fresh digestate also tends to be associated with higher methanogenic activities leading to higher CH_4 emissions [33]. Therefore, the sludge retention cycle of each tank should be taken into account when planning the UAV survey frequency.

For the cake pad, the U10 sensor was not capable of detecting CH_4 when the laser was in nadir position, which might be due to the low reflectance of the cake pad surface or CH_4 emissions being low and localized. The ideal measurement conditions based on sensor capability for CH_4 emissions from cake pads require horizontal laser orientation, flight heights below 2 m above the cake pad surface and stable weather conditions with wind speeds below 3 m s^{-1}. Ideally the survey should be conducted when the cake pad is being manipulated as this is the time when highest emissions and a higher capability of CH_4 detection by the U10 sensor are expected. However, both steady emissions and emissions during cake pad movements need to be understood to define intervention strategies. For enhancement calculation, recorded concentrations need to be either vertical laser path integrated concentrations or horizontally integrated at different heights. The later would require the U10 laser reflecting on a surface located around the perimeter of the cake pad, with sufficient height (approximately 50 m) to take the necessary measurements, and it is therefore impractical. Measurements thus collected will not be useful for flux estimations. However, the recorded path integrated CH_4 measurements indicated that a layer of low methane concentration was present above the cake pad. When it comes to the identification of sources and CH_4 enhancement estimations (Objective 2), the framework presented here gives an asset level (e.g., digester level scale) estimation of enhancement values. This is a step forward over current common reporting practice that rely on activity data and EFs. These enhancement results can also be used in mass balance calculations by incorporating wind vector normalization to the sampled upwind and downwind planes and converting ppm measurements to g m^{-3}. The framework relies on multiple assumptions; emission being continuous throughout the data collection period, stable wind conditions, CH_4 flowing into and out from the specified volume only through upwind and downwind surfaces that will lead to bias in overall enhancement estimations at asset level. Further refinement, calibration and validation is required to move the conceptual design of the framework to an operational stage that promotes uptake across multiple WWTPs. In addition, non-positive enhancements need to be interpreted carefully as they can indicate (i) inability of the U10 to capture the vertical plume extent, (ii) that the emissions are significantly smaller than those from external sources (e.g., gas bags) or (iii) there is CH_4 dispersion from sides and top of the mass balance box considered for the enhancement estimation.

Note that the use of path normalized concentrations would not help establish asset specific guidelines for UAV-U10 based CH_4 monitoring, as the objective is to detect the maximum enhancement values that each asset is responsible for. Emissions from each asset could have different plume configurations, and therefore different heights are required to determine the maximum enhancement. This is in addition to sensor limitations and safety requirements. For example, anaerobic digesters required flights at 30 m height whereas digestate storage tanks required flights at low altitudes. Hence, path normalized values would not have contributed to identify the assets with the highest emissions or where the emissions are concentrated.

Other factors that would curtail the uptake of the framework for operational purposes are determined by the characteristics of the U10. Its dependence on surface reflectance and laser path limits the use of the framework for the characterization of plumes that extended vertically over more than 50 m. Additionally, DeBruyn et al. [34] stated that there could be biases in the linearity between absorption and detected measurement for path integrated concentrations < 50 ppm·m and further research should focus on determining if this limitation is universal or instrument dependent. As of today, and considering the UAV-U10 constraints, the U10 is relatively accurate compared to other sensor types (e.g., electrochemical, solid-state) which are commercially available with required miniaturization.

As far as objective 3 is concerned, results are interpreted here within the context of path integrated CH_4 concentration monitoring for Net Zero compliance. This study has demonstrated that to achieve Net Zero in WWTPs, it is necessary to manage emissions at asset level as quantifications of CH_4 measurements were different for the three assets considered in this study. However, these results cannot be compared with previous work without converting them to mass fluxes

5. Conclusions

This manuscript presents a novel UAV-U10 framework for the characterization of CH_4 enhancement in WWTPs at asset level. Results showed that for anaerobic digesters, interpolation results and overall CH_4 emissions estimations were visually different when handling BQL values as 5 ppm·m compared with the original data. In some instances, this could lead to assets shifting from positive enhancement to non-positive enhancement estimations. Therefore, there is also a need to carefully consider how measurements BQL values are handled when reporting for Net Zero purposes.

Monitoring emissions in open air can be subjected to many uncertainties (e.g., wind conditions). Therefore, there is a need to repeat the work presented here in a controlled environment and with controlled release of CH_4 to assess the reliability (precision and bias) of the method and technology.

Quantification of CH_4 emissions is crucial in order to make informed management decisions and progress towards achieving Net Zero targets. The framework presented here enables the characterization of spatial and temporal variations in concentrations caused by environmental and operational factors. It promotes CH_4 enhancement estimation based on on-site measurements, unlike EF-based approaches recommended by previous studies [4]. It also enables the estimation of enhancements at asset level and could be used to estimate EFs at that scale. Further research is required to extend the methodology presented here to convert enhancement estimations based on path integrated concentrations to mass fluxes, estimate asset specific EFs and compare these values with current EFs used by WWTPs.

Author Contributions: Conceptualization, H.G.K.A., Y.B.-F. and M.R.C.; methodology, H.G.K.A.; software, H.G.K.A. and D.T.; validation, H.G.K.A.; formal analysis, H.G.K.A.; investigation, H.G.K.A.; resources, Y.B.-F., M.R.C., B.S. and D.T.; data curation, H.G.K.A.; writing—original draft preparation, H.G.K.A.; writing—review and editing, B.S., Y.B.-F. and M.R.C.; visualization, H.G.K.A.; supervision, Y.B.-F. and M.R.C.; project administration, M.R.C.; funding acquisition, Y.B.-F. and M.R.C. All authors have read and agreed to the published version of the manuscript.

Funding: This research was funded by Severn Trent Water and the APC was funded by *Remote Sensing*, MDPI.

Data Availability Statement: Data supporting this study are not publicly available due to commercial reasons. Please contact m.rivas-casado@cranfield.ac.uk.

Acknowledgments: We would like to thank the reviewers for the useful comments provided and their constructive criticism. We believe the paper is easier to understand and follow thanks to their input.

Conflicts of Interest: The authors declare no conflict of interest.

Glossary

BQL	Below quantification level
CAW	Carbon accounting workbook
CCC	Committee on Climate Change
CRDS	Cavity ring-down spectroscopy
EF	Emission factor
GHG	Greenhouse gas
GPS	Global positioning system
H	Height
L	Length
NDIR	Nondispersive infrared
RTK	Real-time kinematic
TDLAS	Tuneable diode laser absorption spectroscopy
UAV	Unmanned aerial vehicle
UNFCC	United Nations Framework Convention
VTOL	Vertical take-off and landing
W	Width
WWT	Wastewater treatment
WWTP	Wastewater treatment plant

References

1. Water UK. Ricardo, and Mott MacDonald, "Net Zero 2030 Routemap". 2020, p. 90. Available online: https://www.water.org.uk/routemap2030/wp-content/uploads/2020/11/Water-UK-Net-Zero-2030-Routemap.pdf (accessed on 1 May 2023).
2. Delbeke, J.; Runge-Metzger, A.; Slingenberg, Y.; Werksman, J. The paris agreement. In *Towards a Climate-Neutral Europe Curbing the Trend*; Routledge: London, UK, 2019; pp. 24–45. [CrossRef]
3. National Statistics. *Final UK Greenhouse Gas Emissions National Statistics: 1990 to 2020*; Department Business, Energy & Industrial Strategy: London, UK, 2020; p. 47. Available online: https://www.ipcc-nggip.iges.or.jp/public/wetlands/index.html;%0Ahttps://www.gov.uk/government/uploads/system/uploads/attachment_data/file/295968/20140327_2013_UK_Greenhouse_Gas_Emissions_Provisional_Figures.pdf (accessed on 1 May 2023).

4. UKWIR. *Quantifying and Reducing Direct Greenhouse Gas Emissions from Waste and Water Treatment Process*; UKWIR: London, UK, 2020.
5. IPCC. Chapter 6: Wastewater Treatment and Discharge. In *2006 IPCC Guidelines for National Greenhouse Gas Inventories*; IPCC: Geneva, Switzerland, 2006; Volume 5, pp. 1–56.
6. Daelman, M.R.; van Voorthuizen, E.M.; van Dongen, U.G.; Volcke, E.I.; van Loosdrecht, M.C. Methane emission during municipal wastewater treatment. *Water Res.* **2012**, *46*, 3657–3670. [CrossRef]
7. Nathan, B.J.; Golston, L.M.; O'brien, A.S.; Ross, K.; Harrison, W.A.; Tao, L.; Lary, D.J.; Johnson, D.R.; Covington, A.N.; Clark, N.N.; et al. Near-Field Characterization of Methane Emission Variability from a Compressor Station Using a Model Aircraft. *Environ. Sci. Technol.* **2015**, *49*, 7896–7903. [CrossRef] [PubMed]
8. Allen, G.; Pitt, J.; Hollingsworth, P.; Mead, I.; Kabbabe, K.; Roberts, G.; Percival, C. *Measuring Landfill Methane Emissions Using Unmanned Aerial Systems: Field Trial and Operational Guidance*; Environment Agency: Bristol, UK, 2015.
9. Yang, S.; Talbot, R.W.; Frish, M.B.; Golston, L.M.; Aubut, N.F.; Zondlo, M.A.; Gretencord, C.; McSpiritt, J. Natural Gas Fugitive Leak Detection Using an Unmanned Aerial Vehicle: Measurement System Description and Mass Balance Approach. *Atmosphere* **2018**, *9*, 383. [CrossRef]
10. Delre, A.; Mønster, J.; Scheutz, C. Greenhouse gas emission quantification from wastewater treatment plants, using a tracer gas dispersion method. *Sci. Total Environ.* **2017**, *605-606*, 258–268. [CrossRef] [PubMed]
11. Ren, H.; Zhao, Y.; Xiao, W.; Hu, Z. A review of UAV monitoring in mining areas: Current status and future perspectives. *Int. J. Coal Sci. Technol.* **2019**, *6*, 320–333. [CrossRef]
12. Shah, A.; Pitt, J.; Kabbabe, K.; Allen, G. Suitability of a non-dispersive infrared methane sensor package for flux quantification using an unmanned aerial vehicle. *Sensors* **2019**, *19*, 4705. [CrossRef] [PubMed]
13. Webster, R.; Oliver, M.A. *Geostatistics for Environmental Scientists*, 2nd ed.; John Wiley & Sons: New York, NY, USA, 2007.
14. Neumann, P.P.; Kohlhoff, H.; Hüllmann, D.; Krentel, D.; Kluge, M.; Dzierliński, M.; Lilienthal, A.J.; Bartholmai, M. Aerial-based gas tomography–from single beams to complex gas distributions. *Eur. J. Remote Sens.* **2019**, *52*, 2–16. [CrossRef]
15. AiLF. User Manual UAV Based Laser Methane Leakage Detector. AiLF (Shandong) Instruments Inc. 2019. Available online: https://www.manualslib.com/manual/1860232/Ailf-U10.html (accessed on 1 May 2023).
16. Driessen, W.; Snelson, P.; Chadha, M. Advanced Reject Water Treatment. 2014, pp. 1–6. Available online: https://waterprojectsonline.com/wp-content/uploads/case_studies/2012/Minworth-STW-Anammox-Plant-2012.pdf (accessed on 1 July 2023).
17. Esri. 'Imagery' [basemap]. Scale Not Given. 'World Imagery'. 12 December 2009. Available online: https://www.arcgis.com/home/item.html?id=10df2279f9684e4a9f6a7f08febac2a9 (accessed on 1 May 2023).
18. Shaw, J.T.; Shah, A.; Yong, H.; Allen, G. Methods for quantifying methane emissions using unmanned aerial vehicles: A review. *Philos. Trans. R. Soc. A Math. Phys. Eng. Sci.* **2021**, *379*, 20200450. [CrossRef]
19. Wheeler, M.D.; Newman, S.M.; Orr-Ewing, A.J.; Ashfold, M.N.R. Cavity ring-down spectroscopy. *J. Chem. Soc. Faraday Trans.* **1998**, *94*, 337–351. [CrossRef]
20. Martinez, B.; Miller, T.W.; Yalin, A.P. Cavity Ring-Down Methane Sensor for Small Unmanned Aerial Systems. *Sensors* **2020**, *20*, 454. [CrossRef] [PubMed]
21. DJI. MATRICE 300 RTK-Specifications-DJI. Available online: https://www.dji.com/uk/matrice-300/specs (accessed on 1 November 2022).
22. DJI. Matrice 600 Pro. Available online: https://www.dji.com/uk/matrice600-pro (accessed on 1 July 2023).
23. Baker Hughes. Lumen Terrain User's Manual. Baker Hughes. 2019. Available online: https://manuals.plus/m/3635b9330db4c3aaf53bb2bf1efab08ebd71213a7446afb21db2df1666d9bf59.pdf (accessed on 1 May 2023).
24. Yi, W.Y.; Lo, K.M.; Mak, T.; Leung, K.S.; Leung, Y.; Meng, M.L. A survey of wireless sensor network based air pollution monitoring systems. *Sensors* **2015**, *15*, 31392–31427. [CrossRef] [PubMed]
25. Information, T.; Sensors, M.G. Technical Information for TGS2611 an ISO9001 and 14001 Company Technical Information for Methane Gas Sensors Technical Information for TGS2611. pp. 1–13. Available online: https://asset.conrad.com/media10/add/160267/c1/-/en/000183302DS01/datenblatt-183302-figaro-gas-sensor-tgs-2611-passend-fuer-gase-methan-o-x-h-92-mm-x-78-mm.pdf (accessed on 1 May 2023).
26. Carslaw, D. *The Openair Manual—Open-Source Tools for Analysing Airpollution Data*; Manual for Version 2.6-6; University of York: York, UK, 2019; Available online: https://davidcarslaw.com/files/openairmanual.pdf (accessed on 1 May 2023).
27. Allen, G.; Gallagher, M.; Hollingsworth, P.; Illingworth, S.; Kabbabe, K.; Percival, C. *Feasibility of Aerial Measurements of Methane Emissions from Landfills*; Environment Agency: Bristol, UK, 2014.
28. Ermolaev, E.; Sundberg, C.; Pell, M.; Smårs, S.; Jönsson, H. Effects of moisture on emissions of methane, nitrous oxide and carbon dioxide from food and garden waste composting. *J. Clean. Prod.* **2019**, *240*, 118165. [CrossRef]
29. Fane, S.; Nocker, A.; Vale, P.; Casado, M.R.; Cartmell, E.; Harris, J.; Fernández, Y.B.; Tyrrel, S. Characterisation and control of the biosolids storage environment: Implications for E. coli dynamics. *Sci. Total Environ.* **2020**, *752*, 141705. [CrossRef] [PubMed]
30. Aldhafeeri, T.; Tran, M.-K.; Vrolyk, R.; Pope, M.; Fowler, M. A Review of Methane Gas Detection Sensors: Recent Developments and Future Perspectives. *Inventions* **2020**, *5*, 28. [CrossRef]
31. Wang, C.; Yin, L.; Zhang, L.; Xiang, D.; Gao, R. Metal Oxide Gas Sensors: Sensitivity and Influencing Factors. *Sensors* **2010**, *10*, 2088–2106. [CrossRef]

32. Duan, Y.-F.; Reinsch, S.; Ambus, P.; Elsgaard, L.; Petersen, S.O. Activity of Type I Methanotrophs Dominates under High Methane Concentration: Methanotrophic Activity in Slurry Surface Crusts as Influenced by Methane, Oxygen, and Inorganic Nitrogen. *J. Environ. Qual.* **2017**, *46*, 767–775. [CrossRef]
33. Maldaner, L.; Wagner-Riddle, C.; VanderZaag, A.C.; Gordon, R.; Duke, C. Methane emissions from storage of digestate at a dairy manure biogas facility. *Agric. For. Meteorol.* **2018**, *258*, 96–107. [CrossRef]
34. DeBruyn, Z.J.; Wagner-Riddle, C.; VanderZaag, A. Assessment of Open-path Spectrometer Accuracy at Low Path-integrated Methane Concentrations. *Atmosphere* **2020**, *11*, 184. [CrossRef]